

A-posteriori-steered p -robust multigrid and domain decomposition methods with optimal step-sizes for mixed finite element discretizations of elliptic problems*

Ani Miraçi[¶] Jan Papež^{||} Martin Vohralík^{†‡} Ivan Yotov[§]

June 17, 2024

Abstract

In this work, we develop algebraic solvers for linear systems arising from the discretization of second-order elliptic problems by saddle-point mixed finite element methods of arbitrary polynomial degree $p \geq 0$. We present a multigrid and a two-level domain decomposition approach in two or three space dimensions, which are steered by their respective a posteriori estimators of the algebraic error. First, we extend the results of [A. Miraçi, J. Papež, and M. Vohralík, *SIAM J. Sci. Comput.* 43 (2021), S117–S145] to the mixed finite element setting. Extending the multigrid procedure itself is rather natural. To obtain analogous theoretical results, however, a multilevel stable decomposition of the velocity space is needed. In two space dimensions, we can treat the velocity space as the curl of a stream-function space, for which the previous results apply. In three space dimensions, we design a novel stable decomposition by combining a one-level high-order local stable decomposition of [Chaumont-Frelet and Vohralík, *SIAM J. Numer. Anal.* 61 (2023), 1783–1818] and a multilevel lowest-order stable decomposition of [Hiptmair, Wu, and Zheng, *Numer. Math. Theory Methods Appl.* 5 (2012), 297–332]. This allows us to prove that our multigrid solver contracts the algebraic error at each iteration and, simultaneously, that the associated a posteriori estimator is efficient. A p -robust contraction is shown in two space dimensions. Next, we use this multilevel methodology to define a two-level domain decomposition method where the subdomains consist of overlapping patches of coarse-level elements sharing a common coarse-level vertex. We again establish a (p -robust) contraction of the solver and efficiency of the a posteriori estimator. Numerical results presented both for the multigrid approach and the domain decomposition method confirm the theoretical findings.

Key words: mixed finite element method, multigrid method, Schwarz method, a posteriori error estimate, stable decomposition, polynomial-degree robustness

1 Introduction

In many physical problems studying fluid flows, the main focus is to obtain an accurate representation of the velocity variable. While different discretization methods can be used to approximate the

*This project has received funding from Austrian Science Fund (FWF) project [10.55776/F65](#) (SFB F65 “Taming complexity in PDE systems”), the scientific mobility grant Christiana Hörbiger 2021, Czech Academy of Sciences RVO 67985840, the Grant Agency of the Czech Republic grant no. 23-06159S, Inria Paris Visiting Professorship, NSF grants DMS 2111129 and DMS 241068. Jan Papež is a member of Nečas Center for Mathematical Modeling.

[¶]TU Wien, Institute of Analysis and Scientific Computing, Wiedner Hauptstr. 8-10/E101/4, 1040 Vienna, Austria

^{||}Institute of Mathematics, Czech Academy of Sciences, Žitná 25, 115 67 Prague, Czech Republic

[†]Inria, 2 rue Simone Iff, 75589 Paris, France

[‡]CERMICS, Ecole des Ponts, 77455 Marne-la-Vallée, France

[§]Department of Mathematics, University of Pittsburgh, Pittsburgh, PA 15260 USA

fluid velocity, the mixed finite element method, see e.g., Boffi, Brezzi, and Fortin [3] and the references therein, has been one of the most attractive approaches because of the accuracy, robustness, and instantaneous local mass conservation it provides. In order to benefit from these advantages, suitable algebraic iterative solvers should also be considered. One difficulty is that some common formulations lead to a saddle-point form with an indefinite linear system, see e.g., Benzi, Golub, and Liesen [2] or Brenner [5] and the references therein.

Amidst a large class of algebraic iterative solvers, multilevel methods such as multigrid methods and domain decomposition methods with a coarse-grid solve have proven to be efficient, accurate, and robust in many different applications. For a domain decomposition approach in the setting of mixed discretizations, we refer to, e.g., the works of Glowinski and Wheeler [21], Cowsar, Mandel, and Wheeler [14], and more recently to, e.g., Jayadharan, Khattatov, and Yotov [28]. Another possible approach is that of multigrid methods, see, e.g., Brenner [4] for an optimal multigrid in a lowest-order Raviart–Thomas setting, Wheeler and Yotov [50] for a non-matching grids setting, Schöberl and Zulehner [44], Takacs and Zulehner [46], or Brenner, Oh, and Sung [6] for all-at-once multigrid methods, where all the unknowns are treated simultaneously and the error analysis is similar to that of non-conforming methods since mesh-dependent inner products are used. An abstract framework for multigrid convergence in Raviart–Thomas spaces is developed in Arnold, Falk, and Winther [1]. In some cases, it is possible to rewrite the problem such that, if one first constructs a suitable initial approximation of the velocity which satisfies a divergence constraint, then only a symmetric and positive definite divergence-free problem remains to be solved. This approach was followed in Chavent et al. [12] and then later in Ewing and Wang [19, 20], Mathew [32], Hiptmair and Hoppe [24], or Cai et al. [9] to develop multilevel solvers for nested spaces. We adopt the same setting here.

In this work, we present two solvers for mixed finite element discretizations: a multigrid solver and a domain decomposition solver. Our analysis is however, unified, since our domain decomposition solver fits within our multigrid setting. One iteration of our multigrid solver consists in a V-cycle with zero pre- and solely one post-smoothing step with additive Schwarz (block-Jacobi) as a smoother and *optimal levelwise step-sizes* given by line search at the error correction stage, see e.g., Heinrichs [23]. This, as in Miraçi, Papež, and Vohralík [34] for conforming finite elements, leads to the following *Pythagorean formula* for the decrease of the algebraic error in each step:

$$\|\mathbf{K}^{-1/2}(\mathbf{u}_J - \mathbf{u}_J^{i+1})\|^2 = \|\mathbf{K}^{-1/2}(\mathbf{u}_J - \mathbf{u}_J^i)\|^2 - \underbrace{\sum_{j=0}^J (\lambda_j^i \|\mathbf{K}^{-1/2} \boldsymbol{\rho}_j^i\|)^2}_{(\eta_{\text{alg}}^i)^2}, \quad (1)$$

where i is the solver iteration counter, \mathbf{K} is the diffusion tensor, $j \in \{0, \dots, J\}$ is the level counter, \mathbf{u}_J is the (unknown) exact algebraic solution, \mathbf{u}_J^i denotes the current iterate, \mathbf{u}_J^{i+1} is the iterate that is being computed via $\boldsymbol{\rho}_j^i$, the levelwise smoothing corrections, and λ_j^i are the levelwise optimal step-sizes. In particular, formula (1) gives a *computable levelwise decrease* of the (square of the) algebraic error by the factors $(\lambda_j^i \|\mathbf{K}^{-1/2} \boldsymbol{\rho}_j^i\|)^2$. This naturally defines a built-in (no additional construction is required) a posteriori estimator η_{alg}^i , representing a guaranteed lower bound of the algebraic error $\|\mathbf{K}^{-1/2}(\mathbf{u}_J - \mathbf{u}_J^i)\|$ on step i . In this sense, we refer to the present algebraic solver as *a-posteriori steered*. Moreover, one can use the block-smoothing structure of the solver and the definitions of λ_j^i to further rewrite the estimator on the algebraic error as

$$(\eta_{\text{alg}}^i)^2 = \|\mathbf{K}^{-1/2} \boldsymbol{\rho}_0^i\|^2 + \sum_{j=1}^J \lambda_j^i \sum_{a \in \mathcal{V}_j} \|\mathbf{K}^{-1/2} \boldsymbol{\rho}_{j,a}^i\|_{\omega_j^a}^2, \quad (2)$$

which localizes our estimate on the algebraic error with respect to mesh levels as well as with respect to vertex patches ω_j^a on each level. This multigrid methodology is then used to define a two-level *domain decomposition* method, where the subdomains are the overlapping patches of the coarsest level, a fine level solve is applied on each of them, and a coarse solver ensures uniform contraction. In particular, our methods do not need any additional smoothing steps or any damping/relaxation parameters which might require tuning. Details form the content of Theorem 6.1.

Further main results read as follows. First, we prove that the introduced multigrid solver as well as the domain decomposition solver *contract* the algebraic error at each iteration, i.e.,

$$\|\mathbf{K}^{-1/2}(\mathbf{u}_J - \mathbf{u}_J^{i+1})\| \leq \alpha \|\mathbf{K}^{-1/2}(\mathbf{u}_J - \mathbf{u}_J^i)\|, \quad 0 < \alpha < 1, \quad (3)$$

see Theorem 6.3 for details. Second, we show that the associated a posteriori estimators are *efficient* in that

$$\eta_{\text{alg}}^i \geq \beta \|\mathbf{K}^{-1/2}(\mathbf{u}_J - \mathbf{u}_J^i)\|, \quad 0 < \beta < 1, \quad (4)$$

see Theorem 6.2. In fact, proving the two above results is equivalent, owing to the connection between solvers and estimators as described by the Pythagorean formula (1). In two space dimensions, we can prove that the above results hold independently of the polynomial degree p , i.e., *p-robustly*.

A crucial ingredient needed for our analysis is a (polynomial-degree-robust) *multilevel stable splitting*, which is given in Miraçi, Papež, and Vohralík [33] by combining the p -robust one-level stable splitting achieved in Schöberl et al. [43] and a multilevel piecewise affine stable splitting from Xu, Chen, and Nocketto [52]. In order to adapt this to our case, in two space dimensions, we use the connection between discrete stream-function spaces and discrete velocity spaces. In three space dimensions, we rely instead on the one-level patch-wise decomposition of a divergence-free velocity owing to Chaumont-Frelet and Vohralík [10] together with the property that a divergence-free velocity has a vector potential which we can then decompose in a stable way over the levels and patches for the lowest-order case by following Hiptmair, Wu, and Zheng [25]. We emphasize that the analysis for both the multigrid solver and the domain decomposition method rely on the same arguments and that the results hold for quasi-uniform meshes as well as possibly highly graded ones.

This work is organized as follows. In Section 2 we present the model problem and its mixed finite element discretization. The multilevel setting and assumptions used in our theory are collected in Section 3. In Section 4 we present the a-posteriori-steered multigrid solver with its associated a posteriori estimator of the algebraic error and in Section 5 we similarly present the domain decomposition method with the associated a posteriori estimator. Our main results are summarized in Section 6 and the numerical experiments are presented in Section 7. In Section 8, we collect intermediate results, which can be of independent interest. They namely allow us to obtain the stable decomposition needed as crucial ingredient of our main results. Finally, proofs of the main theorem form the content of Section 9 and some concluding remarks are given in Section 10.

2 Model elliptic problem and its mixed finite element discretization

Consider an elliptic partial differential equation in a mixed form modeling, for example, the single phase flow in porous media. Let $\Omega \subset \mathbb{R}^d$, $d = 2, 3$, be a polytopal domain with Lipschitz boundary that is homotopic to a ball.

2.1 Model elliptic problem

The governing equations we are interested in are

$$\mathbf{u} = -\mathbf{K}\nabla\gamma, \quad \nabla\cdot\mathbf{u} = f \quad \text{in } \Omega, \quad \mathbf{u}\cdot\mathbf{n} = 0 \quad \text{on } \partial\Omega, \quad (5)$$

where γ is the fluid pressure, \mathbf{u} is the Darcy velocity, f is the source term such that $(f, 1) = 0$ in Ω , \mathbf{n} is the outward normal vector on $\partial\Omega$, and \mathbf{K} is a bounded, symmetric, and uniformly positive definite tensor representing the rock permeability divided by the fluid viscosity. More precisely, we assume that there exist $0 < \Lambda_{\min} \leq \Lambda_{\max}$ such that all eigenvalues of \mathbf{K} belong to the interval $[\Lambda_{\min}, \Lambda_{\max}]$. The homogeneous Neumann boundary condition in (5) is assumed merely for simplicity of exposition; inhomogeneous and mixed boundary conditions can be considered as well.

2.2 Function spaces and weak formulations

Define the spaces

$$\mathbf{V} := \mathbf{H}_0(\text{div}; \Omega) := \{\mathbf{v} \in \mathbf{H}(\text{div}; \Omega), \mathbf{v}\cdot\mathbf{n} = 0 \text{ on } \partial\Omega \text{ in appropriate sense}\}, \quad (6a)$$

$$W := L_0^2(\Omega) := \{w \in L^2(\Omega), (w, 1) = 0 \text{ in } \Omega\}. \quad (6b)$$

Let $(\cdot, \cdot)_S$ and $\|\cdot\|_S$, $S \subset \mathbb{R}^d$, be the $L^2(S)$ inner product and norm, respectively, where we omit the subscript if $S = \Omega$. The so-called mixed weak formulation of (5), see e.g., Boffi, Brezzi, and Fortin [3], is: find $\mathbf{u} \in \mathbf{V}$ and $\gamma \in W$ such that

$$(\mathbf{K}^{-1}\mathbf{u}, \mathbf{v}) - (\gamma, \nabla\cdot\mathbf{v}) = 0 \quad \forall \mathbf{v} \in \mathbf{V}, \quad (7a)$$

$$(\nabla\cdot\mathbf{u}, w) = (f, w) \quad \forall w \in W. \quad (7b)$$

For $g \in L_0^2(\Omega)$, let

$$\mathbf{V}^g := \{\mathbf{v} \in \mathbf{V} : \nabla\cdot\mathbf{v} = g\} \quad (8)$$

Problem (7) can be written equivalently via the so-called dual weak formulation: find $\mathbf{u} \in \mathbf{V}^f$ such that

$$(\mathbf{K}^{-1}\mathbf{u}, \mathbf{v}) = 0 \quad \forall \mathbf{v} \in \mathbf{V}^0. \quad (9)$$

2.3 Mixed finite element discretization

In order to discretize the model problem (7), we first introduce a shape-regular mesh \mathcal{T}_J , partitioning Ω into d -simplices (triangles or tetrahedra). Then, we fix an integer $p \geq 0$ which denotes the polynomial degree used in our mixed finite element (MFE) spaces $\mathbf{V}_J \times W_J \subset \mathbf{V} \times W$. For our setting, we shall work with the Raviart–Thomas (\mathbf{RT}) spaces, see Raviart and Thomas [39] for two space dimensions, Nédélec [38] for three space dimensions, or Boffi, Brezzi, and Fortin [3, Section 2.3.1]. We introduce the space $\mathbb{P}_p(K)$ of scalar-valued polynomials of degree p on an element $K \in \mathcal{T}_J$ and denote by $\mathbf{RT}_p(K) := [\mathbb{P}_p(K)]^d + \mathbb{P}_p(K)\mathbf{x}$ the Raviart–Thomas(–Nédélec) space on $K \in \mathcal{T}_J$. Define $\mathbf{RT}_p(\mathcal{T}_J) := \{\mathbf{v}_J \in \mathbf{L}^2(\Omega), \mathbf{v}_J|_K \in \mathbf{RT}_p(K) \forall K \in \mathcal{T}_J\}$ and

$$\mathbf{V}_J := \{\mathbf{v}_J \in \mathbf{V}, \mathbf{v}_J|_K \in \mathbf{RT}_p(K) \forall K \in \mathcal{T}_J\}, \quad (10)$$

$$W_J := \{w_J \in W, w_J|_K \in \mathbb{P}_p(K) \forall K \in \mathcal{T}_J\}. \quad (11)$$

We search for $\mathbf{u}_J \in \mathbf{V}_J$ and $\gamma_J \in W_J$ such that

$$(\mathbf{K}^{-1}\mathbf{u}_J, \mathbf{v}_J) - (\gamma_J, \nabla\cdot\mathbf{v}_J) = 0 \quad \forall \mathbf{v}_J \in \mathbf{V}_J, \quad (12a)$$

$$(\nabla\cdot\mathbf{u}_J, w_J) = (f, w_J) \quad \forall w_J \in W_J. \quad (12b)$$

Denoting $\mathbf{V}_J^g := \{\mathbf{v}_J \in \mathbf{V}_J : (\nabla \cdot \mathbf{v}_J, w_J) = (g, w_J) \ \forall w_J \in W_J\}$, the method (12) can again be written equivalently as: find $\mathbf{u}_J \in \mathbf{V}_J^f$ such that

$$(\mathbf{K}^{-1} \mathbf{u}_J, \mathbf{v}_J) = 0 \quad \forall \mathbf{v}_J \in \mathbf{V}_J^0. \quad (13)$$

Remark 2.1 (Other choices of discrete spaces). *Consider the Brezzi–Douglas–Marini (BDM) spaces, see Brezzi, Douglas, and Marini [7], and denote the elementwise divergence-free spaces $\mathbf{BDM}_p^0(K) := \{\mathbf{v} \in \mathbf{BDM}_p(K), \nabla \cdot \mathbf{v} = 0\}$, for all $K \in \mathcal{T}_J$. Let similarly $\mathbf{RT}_p^0(K) := \{\mathbf{v} \in \mathbf{RT}_p(K), \nabla \cdot \mathbf{v} = 0\}$. From Boffi, Brezzi, and Fortin [3, Corollary 2.3.1], one has $\mathbf{RT}_p^0(K) = \mathbf{BDM}_p^0(K)$ for all $K \in \mathcal{T}_J$. Since, after an initial step of constructing a velocity that satisfies the divergence constraint, we only work with divergence-free functions, the results of this work hold also for this choice of mixed finite element spaces.*

3 Hierarchy of meshes and spaces

We introduce here the assumptions on the hierarchy of meshes and the associated hierarchy of spaces used in this manuscript.

3.1 Hierarchy of meshes

To define our solvers, we consider a hierarchy of nested matching simplicial meshes of Ω , $\{\mathcal{T}_j\}_{0 \leq j \leq J}$, $J \geq 1$, where \mathcal{T}_j is a refinement of \mathcal{T}_{j-1} , $1 \leq j \leq J$, and where \mathcal{T}_J has been considered in Section 2.3. For any element $K \in \mathcal{T}_j$, we denote $h_K := \text{diam}(K)$, and we also use $h_j := \max_{K \in \mathcal{T}_j} h_K$. Let $\kappa_{\mathcal{T}} > 0$ denote the shape-regularity parameter, i.e., the smallest constant such that

$$\max_{K \in \mathcal{T}_j} \frac{h_K}{\rho_K} \leq \kappa_{\mathcal{T}} \text{ for all } 0 \leq j \leq J, \quad (14)$$

where ρ_K denotes the diameter of the largest ball inscribed in K .

We will work in one of the two settings corresponding to the two assumptions below. In the first setting, we assume:

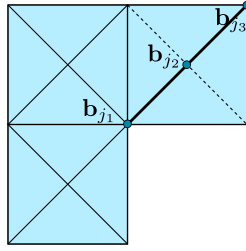
Assumption 3.1 (Mesh quasi-uniformity and refinement strength). *There exists a fixed positive real number $0 < C_{\text{qu}} \leq 1$ such that for all $j \in \{0, \dots, J\}$ and for all $K \in \mathcal{T}_j$, there holds*

$$C_{\text{qu}} h_j \leq h_K \leq h_j. \quad (15)$$

There further exists a fixed positive real number $0 < C_{\text{ref}} \leq 1$ such that for all $j \in \{1, \dots, J\}$, for all $K \in \mathcal{T}_{j-1}$, and all $K^ \in \mathcal{T}_j$ such that $K^* \subset K$, there holds*

$$C_{\text{ref}} h_K \leq h_{K^*} \leq h_K. \quad (16)$$

In the second setting, we assume that our hierarchy is generated from a quasi-uniform coarse mesh \mathcal{T}_0 by a series of bisections, e.g., newest vertex bisection, see, e.g., Stevenson [45] for $d = 2$ and admissible coarse mesh, Karkulik, Pavlicek, and Praetorius [29] for general coarse mesh when $d = 2$, and the recent work Dienes, Gehring, Storn [15] for general coarse mesh when $d \geq 2$. We illustrate in Figure 1 for $d = 2$ how refining one edge of \mathcal{T}_{j-1} , $j \in \{1, \dots, J\}$, leads to a new finer mesh \mathcal{T}_j . Let us now denote by \mathcal{V}_j the set of vertices in \mathcal{T}_j and by $\mathcal{B}_j \subset \mathcal{V}_j$ the set consisting of the new vertex obtained after the bisection together with its two neighbors on the refinement edge. Moreover, let $h_{\mathcal{B}_j}$ be the maximal diameter of elements having a vertex in the set \mathcal{B}_j , for $j \in \{1, \dots, J\}$. We assume:



\mathcal{T}_j obtained by bisection of \mathcal{T}_{j-1}
 neighboring vertices \mathbf{b}_{j1} , \mathbf{b}_{j3} on the refinement edge
 new vertex after refinement \mathbf{b}_{j2}
 $\mathcal{B}_j = \{\mathbf{b}_{j1}, \mathbf{b}_{j2}, \mathbf{b}_{j3}\}$

Figure 1: Illustration of the set \mathcal{B}_j ; the refinement \mathcal{T}_j (dotted lines) of the mesh \mathcal{T}_{j-1} (full lines).

Assumption 3.2 (Coarsest mesh quasi-uniformity and local refinement strength of bisection-generated meshes). *The coarsest mesh \mathcal{T}_0 is a quasi-uniform mesh in the sense of (15), with parameter $0 < C_{\text{qu}}^0 \leq 1$. The (possibly highly graded) conforming mesh \mathcal{T}_J is generated from \mathcal{T}_0 by a series of bisections. There exists a fixed positive real number $0 < C_{\text{loc,qu}} \leq 1$ such that for all $j \in \{1, \dots, J\}$, there holds*

$$C_{\text{loc,qu}} h_{\mathcal{B}_j} \leq h_K \leq h_{\mathcal{B}_j} \quad \forall K \in \mathcal{T}_j \text{ such that a vertex of } K \text{ belongs to } \mathcal{B}_j. \quad (17)$$

3.2 Hierarchy of spaces

To define our solvers, we also consider a hierarchy of nested mixed finite element spaces associated to the nested meshes $\{\mathcal{T}_j\}_{j=0}^J$. First, fix a sequence of non-decreasing polynomial degrees

$$0 \leq p_0 \leq p_1 \leq \dots \leq p_J = p. \quad (18)$$

Then, for $0 \leq j \leq J$, define the levelwise mixed finite element space

$$\mathbf{V}_j := \{\mathbf{v}_j \in \mathbf{V}, \mathbf{v}_j|_K \in \mathbf{RT}_{p_j}(K) \forall K \in \mathcal{T}_j\}. \quad (19)$$

We also define, for $0 \leq j \leq J$, the levelwise divergence-free discrete spaces

$$\mathbf{V}_j^0 := \{\mathbf{v}_j \in \mathbf{V}_j, \nabla \cdot \mathbf{v}_j = 0\}. \quad (20)$$

4 A-posteriori-steered multigrid solver

We can now develop a multigrid solver for iterative approximation of the discrete problem (12) using the introduced multilevel setting.

4.1 Setting for patchwise smoothing

The solver we develop involves solving in each iteration: 1) a global coarse-grid problem (global residual solve); 2) local problems on patches of elements sharing a vertex on all other grids of the hierarchy (block-Jacobi smoothing). We begin with the definition of the patches. Let \mathcal{V}_j be the set of vertices of the mesh \mathcal{T}_j and let \mathcal{V}_K be the set of vertices of an element K of \mathcal{T}_j . Given a vertex $\mathbf{a} \in \mathcal{V}_j$, $j \in \{1, \dots, J\}$, we denote the patch associated to \mathbf{a} by

$$\mathcal{T}_j^{\mathbf{a}} := \{K \in \mathcal{T}_j, \mathbf{a} \in \mathcal{V}_K\}. \quad (21)$$

Denote the corresponding open patch subdomain by $\omega_j^{\mathbf{a}}$. Define the local MFE spaces on $\omega_j^{\mathbf{a}}$ associated with \mathcal{T}_j as

$$\mathbf{V}_j^{\mathbf{a}} := \{\mathbf{v}_j \in \mathbf{V}_j|_{\omega_j^{\mathbf{a}}}, \mathbf{v}_j \cdot \mathbf{n} = 0 \text{ on } \partial\omega_j^{\mathbf{a}}\}. \quad (22)$$

Finally, define

$$\mathbf{V}_j^{\mathbf{a},0} := \{\mathbf{v}_{j,\mathbf{a}} \in \mathbf{V}_j^{\mathbf{a}}, \nabla \cdot \mathbf{v}_{j,\mathbf{a}} = 0\}. \quad (23)$$

Remark 4.1 (Choice of patch subdomains). *Other types of patches can also be considered. For example, in [33], larger patches, obtained by combining all elements in the coarser mesh \mathcal{T}_{j-1} that share a vertex in \mathcal{V}_{j-1} , are also studied. The trade-off is that, though the local problems are larger in size, there are fewer of these larger patches. The theoretical results also apply in this case. For simplicity we limit the presentation here to the above standard vertex patches.*

4.2 Multigrid solver

We now proceed with the definition of the iterative solver.

Algorithm 4.2 (A-posteriori-steered multigrid solver).

1. Initialize $\mathbf{u}_j^0 \in \mathbf{V}_j^f$, e.g., as done in Ewing and Wang [19, Theorem 3.1]. Thus, \mathbf{u}_j^0 has the requested divergence given by f , and all the subsequent corrections will be looked for as divergence-free. Let $i := 0$ and define a tolerance $\tau > 0$.

2. Perform the following steps (a)–(d):

(a) Solve the coarse-grid problem: find the global correction $\boldsymbol{\rho}_0^i \in \mathbf{V}_0^0$ as the solution of the global residual problem

$$(\mathbf{K}^{-1} \boldsymbol{\rho}_0^i, \mathbf{v}_0) = -(\mathbf{K}^{-1} \mathbf{u}_j^i, \mathbf{v}_0) \quad \forall \mathbf{v}_0 \in \mathbf{V}_0^0. \quad (24)$$

Define $\lambda_0^i := 1$ and the coarse-grid update

$$\mathbf{u}_0^i := \mathbf{u}_j^i + \lambda_0^i \boldsymbol{\rho}_0^i \in \mathbf{V}_j^f. \quad (25)$$

(b) For higher levels $1 \leq j \leq J$:

Compute the local corrections $\boldsymbol{\rho}_{j,\mathbf{a}}^i \in \mathbf{V}_j^{\mathbf{a},0}$ as solutions of the patch residual problems, for all level j vertices $\mathbf{a} \in \mathcal{V}_j$,

$$(\mathbf{K}^{-1} \boldsymbol{\rho}_{j,\mathbf{a}}^i, \mathbf{v}_{j,\mathbf{a}})_{\omega_j^{\mathbf{a}}} = -(\mathbf{K}^{-1} \mathbf{u}_{j-1}^i, \mathbf{v}_{j,\mathbf{a}})_{\omega_j^{\mathbf{a}}} \quad \forall \mathbf{v}_{j,\mathbf{a}} \in \mathbf{V}_j^{\mathbf{a},0}. \quad (26)$$

Define the levelwise correction $\boldsymbol{\rho}_j^i \in \mathbf{V}_j^0$ by

$$\boldsymbol{\rho}_j^i := \sum_{\mathbf{a} \in \mathcal{V}_j} \boldsymbol{\rho}_{j,\mathbf{a}}^i. \quad (27)$$

If $\boldsymbol{\rho}_j^i \neq 0$, define the step size by the line search

$$\lambda_j^i := -\frac{(\mathbf{K}^{-1} \mathbf{u}_{j-1}^i, \boldsymbol{\rho}_j^i)}{\|\mathbf{K}^{-1/2} \boldsymbol{\rho}_j^i\|^2}; \quad (28)$$

otherwise set $\lambda_j^i := 1$. Define the level j update

$$\mathbf{u}_j^i := \mathbf{u}_{j-1}^i + \lambda_j^i \boldsymbol{\rho}_j^i \in \mathbf{V}_j^f. \quad (29)$$

(c) Set the next iterate $\mathbf{u}_J^{i+1} := \mathbf{u}_J^i$. Define the a posteriori estimator of the algebraic error

$$\eta_{\text{alg}}^i := \left(\sum_{j=0}^J (\lambda_j^i \|\mathbf{K}^{-1/2} \boldsymbol{\rho}_j^i\|)^2 \right)^{1/2}. \quad (30)$$

(d) If $\eta_{\text{alg}}^i \leq \tau$, then stop the solver. Otherwise set $i := i + 1$ and go to step 2.

4.3 Remarks and basic properties

Remark 4.3 (A-posteriori-steered solver). Note from step 2c of Algorithm 4.2 that both the new solver iterate \mathbf{u}_J^{i+1} and the a posteriori estimator η_{alg}^i of the algebraic error are constructed from the levelwise algebraic residual liftings $\boldsymbol{\rho}_j^i$ and the step size parameters λ_j^i . In this sense, the solver has a built-in algebraic error estimator and we call it a-posteriori-steered.

Remark 4.4 (Compact formulas). The new iterate can be written in the compact form

$$\mathbf{u}_J^{i+1} = \mathbf{u}_J^i + \sum_{j=0}^J \lambda_j^i \boldsymbol{\rho}_j^i \stackrel{(27)}{=} \mathbf{u}_J^i + \boldsymbol{\rho}_0^i + \sum_{j=1}^J \lambda_j^i \sum_{\mathbf{a} \in \mathcal{V}_j} \boldsymbol{\rho}_{j,\mathbf{a}}^i. \quad (31)$$

It is also easy to see that the local updates satisfy for $j \in \{1, \dots, J\}$

$$(\mathbf{K}^{-1} \boldsymbol{\rho}_{j,\mathbf{a}}^i, \mathbf{v}_{j,\mathbf{a}})_{\omega_j^{\mathbf{a}}} = -(\mathbf{K}^{-1} \mathbf{u}_J^i, \mathbf{v}_{j,\mathbf{a}})_{\omega_j^{\mathbf{a}}} - \sum_{m=0}^{j-1} \lambda_m^i (\mathbf{K}^{-1} \boldsymbol{\rho}_m^i, \mathbf{v}_{j,\mathbf{a}})_{\omega_j^{\mathbf{a}}} \quad \forall \mathbf{v}_{j,\mathbf{a}} \in \mathbf{V}_j^{\mathbf{a},0}. \quad (32)$$

Now, we explain through the following lemma that the choice of the step-sizes (28) leads to the best possible decrease of the algebraic error along the direction given by $\boldsymbol{\rho}_j^i$, as also seen and used in, e.g., Heinrichs [23] and [33, 35].

Lemma 4.5 (Optimal step-sizes). For $j \in \{1, \dots, J\}$, the step size λ_j^i defined in (28) satisfies

$$\lambda_j^i = \operatorname{argmin}_{\lambda \in \mathbb{R}} \|\mathbf{K}^{-1/2}(\mathbf{u}_J - (\mathbf{u}_{j-1}^i + \lambda \boldsymbol{\rho}_j^i))\|. \quad (33)$$

Proof. The result follows from determining the minimum of the quadratic function

$$\begin{aligned} \|\mathbf{K}^{-1/2}(\mathbf{u}_J - (\mathbf{u}_{j-1}^i + \lambda \boldsymbol{\rho}_j^i))\|^2 &= \|\mathbf{K}^{-1/2}(\mathbf{u}_J - \mathbf{u}_{j-1}^i)\|^2 - 2\lambda(\mathbf{K}^{-1}(\mathbf{u}_J - \mathbf{u}_{j-1}^i), \boldsymbol{\rho}_j^i) \\ &\quad + \lambda^2 \|\mathbf{K}^{-1/2} \boldsymbol{\rho}_j^i\|^2 \\ &\stackrel{(13)}{=} \|\mathbf{K}^{-1/2}(\mathbf{u}_J - \mathbf{u}_{j-1}^i)\|^2 + 2\lambda(\mathbf{K}^{-1} \mathbf{u}_{j-1}^i, \boldsymbol{\rho}_j^i) \\ &\quad + \lambda^2 \|\mathbf{K}^{-1/2} \boldsymbol{\rho}_j^i\|^2. \end{aligned}$$

Here, in the second equality, we have decisively used that the levelwise correction/algebraic residual lifting $\boldsymbol{\rho}_j^i$ is conforming and divergence-free, i.e., it belongs to the space \mathbf{V}_j^0 , which allows to eliminate the unknown exact solution \mathbf{u}_J from the second term in the development via (13). The above expression implies that

$$\lambda_{\min} = -\frac{(\mathbf{K}^{-1} \mathbf{u}_{j-1}^i, \boldsymbol{\rho}_j^i)}{\|\mathbf{K}^{-1/2} \boldsymbol{\rho}_j^i\|^2}.$$

□

Lemma 4.6 (Norm of the levelwise corrections as sum of norms of the local corrections). *For ρ_j^i given by (26)–(27), $j \in \{1, \dots, J\}$, we have*

$$\sum_{\mathbf{a} \in \mathcal{V}_j} \|\mathbf{K}^{-1/2} \rho_{j,\mathbf{a}}^i\|_{\omega_j^{\mathbf{a}}}^2 \stackrel{(26)}{=} - \sum_{\mathbf{a} \in \mathcal{V}_j} (\mathbf{K}^{-1} \mathbf{u}_{j-1}^i, \rho_{j,\mathbf{a}}^i)_{\omega_j^{\mathbf{a}}} \stackrel{(27)}{=} - (\mathbf{K}^{-1} \mathbf{u}_{j-1}^i, \rho_j^i) \stackrel{(28)}{=} \lambda_j^i \|\mathbf{K}^{-1/2} \rho_j^i\|^2. \quad (34)$$

5 A-posteriori-steered domain decomposition solver

In this section, we present how to adapt the multigrid methodology developed in Section 4 to the domain decomposition setting.

5.1 Setting for subdomains and a coarse grid

We consider a hierarchy of *two* nested matching meshes of Ω , denoted by \mathcal{T}_H and \mathcal{T}_h , where the mesh \mathcal{T}_h is obtained from \mathcal{T}_H by a *sequence* of refinements. More precisely, in the setting of Section 3 with the multilevel mesh hierarchy $\{\mathcal{T}_j\}_{0 \leq j \leq J}$, we take $J \geq 1$, $\mathcal{T}_H := \mathcal{T}_0$, and $\mathcal{T}_h := \mathcal{T}_J$. Only the levels H and h will be used in the algorithm for the domain decomposition, whereas all the levels $0 \leq j \leq J$ will be used in the theoretical analysis.

Denote by \mathcal{V}_H the set of vertices of \mathcal{T}_H and \mathcal{V}_K the set of vertices of an element K of \mathcal{T}_H . For each coarse vertex $\mathbf{a} \in \mathcal{V}_H$, the associated patch of coarse elements sharing \mathbf{a} is $\mathcal{T}_H^{\mathbf{a}} := \{K \in \mathcal{T}_H, \mathbf{a} \in \mathcal{V}_K\}$. Next, we denote the open patch subdomain corresponding to $\mathcal{T}_H^{\mathbf{a}}$ by $\omega_H^{\mathbf{a}}$. These will be used as *subdomains* for the overlapping domain decomposition method. Figure 2 gives an illustration. Define the global and local MFE space as

$$\mathbf{V}_H := \mathbf{V}_0, \quad \mathbf{V}_h := \mathbf{V}_J, \quad \mathbf{V}_H^0 := \mathbf{V}_0^0, \quad \mathbf{V}_h^0 := \mathbf{V}_J^0 \quad (35)$$

and

$$\mathbf{V}_h^{\mathbf{a}} := \{\mathbf{v}_h \in \mathbf{V}_h |_{\omega_H^{\mathbf{a}}} \mathbf{v}_h \cdot \mathbf{n} = 0 \text{ on } \partial\omega_H^{\mathbf{a}}\}. \quad (36)$$

Remark that the latter spaces are restrictions of the fine-mesh MFE space \mathbf{V}_J on the subdomains $\omega_H^{\mathbf{a}}$ with homogeneous Neumann boundary conditions on the whole boundary of the subdomain $\omega_H^{\mathbf{a}}$. Finally, define their divergence-free subspaces as

$$\mathbf{V}_h^{\mathbf{a},0} := \{\mathbf{v}_{h,\mathbf{a}} \in \mathbf{V}_h^{\mathbf{a}}, \nabla \cdot \mathbf{v}_{h,\mathbf{a}} = 0\}. \quad (37)$$

5.2 Domain decomposition solver: overlapping additive Schwarz with a coarse-grid solve

Our domain decomposition solver is similar to the multilevel Algorithm 4.2 in the case of two levels only. It reads:

Algorithm 5.1 (A-posteriori-steered additive Schwarz domain decomposition solver).

1. Initialize $\mathbf{u}_h^0 \in \mathbf{V}_h^f$, e.g., as done in Ewing and Wang [19, Theorem 3.1]. Let $i := 0$ and define a tolerance $\tau > 0$.
2. Perform the following steps (a)–(d):

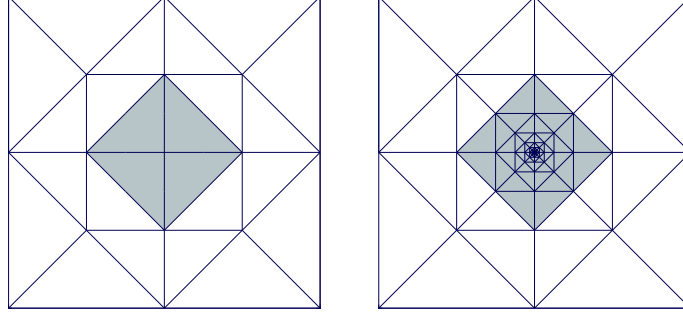


Figure 2: Patch in the two-level overlapping additive Schwarz method: coarse grid \mathcal{T}_H (left), fine grid \mathcal{T}_h (right). The highlighted patch consists of four coarse elements of \mathcal{T}_H which share a vertex and form a subdomain. The subdomains (coarse patches) are discretized with the fine grid \mathcal{T}_h .

- (a) Solve the coarse-grid problem: find the global correction $\boldsymbol{\rho}_H^i \in \mathbf{V}_H^0$ as the solution of the global residual problem

$$(\mathbf{K}^{-1}\boldsymbol{\rho}_H^i, \mathbf{v}_H) = -(\mathbf{K}^{-1}\mathbf{u}_H^i, \mathbf{v}_H) \quad \forall \mathbf{v}_H \in \mathbf{V}_H^0. \quad (38)$$

Define the coarse-grid update

$$\mathbf{u}_H^i := \mathbf{u}_h^i + \boldsymbol{\rho}_H^i \in \mathbf{V}_h^f. \quad (39)$$

- (b) Compute the local corrections $\boldsymbol{\rho}_{h,\mathbf{a}}^i \in \mathbf{V}_h^{\mathbf{a},0}$ as solutions of the subdomain residual problems, for all coarse mesh vertices $\mathbf{a} \in \mathcal{V}_H$,

$$(\mathbf{K}^{-1}\boldsymbol{\rho}_{h,\mathbf{a}}^i, \mathbf{v}_{h,\mathbf{a}})_{\omega_H^{\mathbf{a}}} = -(\mathbf{K}^{-1}\mathbf{u}_H^i, \mathbf{v}_{h,\mathbf{a}})_{\omega_H^{\mathbf{a}}} \quad \forall \mathbf{v}_{h,\mathbf{a}} \in \mathbf{V}_h^{\mathbf{a},0}. \quad (40)$$

Define the overall correction $\boldsymbol{\rho}_h^i \in \mathbf{V}_h^0$ by

$$\boldsymbol{\rho}_h^i := \sum_{\mathbf{a} \in \mathcal{V}_H} \boldsymbol{\rho}_{h,\mathbf{a}}^i. \quad (41)$$

If $\boldsymbol{\rho}_h^i \neq 0$, define the optimal step size by

$$\lambda_h^i := -\frac{(\mathbf{K}^{-1}\mathbf{u}_H^i, \boldsymbol{\rho}_h^i)}{\|\mathbf{K}^{-1/2}\boldsymbol{\rho}_h^i\|^2}; \quad (42)$$

otherwise set $\lambda_h^i := 1$.

- (c) Set the next iterate

$$\mathbf{u}_h^{i+1} := \mathbf{u}_H^i + \lambda_h^i \boldsymbol{\rho}_h^i \in \mathbf{V}_h^f. \quad (43)$$

Define the a posteriori estimator of the algebraic error

$$\eta_{\text{alg}}^i := \left(\|\mathbf{K}^{-1/2}\boldsymbol{\rho}_H^i\|^2 + (\lambda_h^i \|\mathbf{K}^{-1/2}\boldsymbol{\rho}_h^i\|)^2 \right)^{1/2}. \quad (44)$$

- (d) If $\eta_{\text{alg}}^i \leq \tau$, then stop the solver. Otherwise set $i := i + 1$ and go to step 2.

Similarly to Lemma 4.6, we also have here:

Lemma 5.2 (Norm of the overall correction as sum of norms of the subdomain corrections). *For $\boldsymbol{\rho}_h^i$ given by (40)–(41), we have*

$$\sum_{\mathbf{a} \in \mathcal{V}_H} \|\mathbf{K}^{-1/2}\boldsymbol{\rho}_{h,\mathbf{a}}^i\|_{\omega_H^{\mathbf{a}}}^2 \stackrel{(40)}{=} - \sum_{\mathbf{a} \in \mathcal{V}_H} (\mathbf{K}^{-1}\mathbf{u}_H^i, \boldsymbol{\rho}_{h,\mathbf{a}}^i)_{\omega_H^{\mathbf{a}}} \stackrel{(41)}{=} -(\mathbf{K}^{-1}\mathbf{u}_H^i, \boldsymbol{\rho}_h^i) \stackrel{(42)}{=} \lambda_h^i \|\mathbf{K}^{-1/2}\boldsymbol{\rho}_h^i\|^2. \quad (45)$$

6 Main results

We now present our main results for the multigrid solver of Algorithm 4.2 and the domain decomposition method of Algorithm 5.1. To unify the presentation, we suitably equivalently use the symbols J and h and similarly for 0 and H .

6.1 Error representation on each solver step

First, we present an important error reduction property of the solvers, following as in [34, Theorem 4.7].

Theorem 6.1 (Error representation on each solver step). *There holds*

$$\|\mathbf{K}^{-1/2}(\mathbf{u}_J - \mathbf{u}_J^{i+1})\|^2 = \|\mathbf{K}^{-1/2}(\mathbf{u}_J - \mathbf{u}_J^i)\|^2 - (\eta_{\text{alg}}^i)^2. \quad (46)$$

Moreover, the above formula can be localized patch-wise and levelwise by rewriting the a posteriori estimator of the algebraic error for Algorithm 4.2 as

$$(\eta_{\text{alg}}^i)^2 = \|\mathbf{K}^{-1/2}\boldsymbol{\rho}_0^i\|^2 + \sum_{j=1}^J \lambda_j^i \sum_{\mathbf{a} \in \mathcal{V}_j} \|\mathbf{K}^{-1/2}\boldsymbol{\rho}_{j,\mathbf{a}}^i\|_{\omega_j^{\mathbf{a}}}^2, \quad (47)$$

and, for Algorithm 5.1, as

$$(\eta_{\text{alg}}^i)^2 = \|\mathbf{K}^{-1/2}\boldsymbol{\rho}_H^i\|^2 + \lambda_h^i \sum_{\mathbf{a} \in \mathcal{V}_H} \|\mathbf{K}^{-1/2}\boldsymbol{\rho}_{h,\mathbf{a}}^i\|_{\omega_H^{\mathbf{a}}}^2. \quad (48)$$

Proof. We first present the proof in the case of Algorithm 5.1. The error representation (46) is obtained by using the definition of optimal step-sizes and visiting the levels from fine to coarse

$$\begin{aligned} \|\mathbf{K}^{-1/2}(\mathbf{u}_J - \mathbf{u}_h^{i+1})\|^2 &\stackrel{(43)}{=} \|\mathbf{K}^{-1/2}(\mathbf{u}_J - \mathbf{u}_H^i)\|^2 - 2\lambda_h^i(\mathbf{K}^{-1}(\mathbf{u}_J - \mathbf{u}_H^i), \boldsymbol{\rho}_h^i) + (\lambda_h^i \|\mathbf{K}^{-1/2}\boldsymbol{\rho}_h^i\|)^2 \\ &\stackrel{(13)}{=} \|\mathbf{K}^{-1/2}(\mathbf{u}_J - \mathbf{u}_H^i)\|^2 + 2\lambda_h^i(\mathbf{K}^{-1}\mathbf{u}_H^i, \boldsymbol{\rho}_h^i) + (\lambda_h^i \|\mathbf{K}^{-1/2}\boldsymbol{\rho}_h^i\|)^2 \\ &\stackrel{(42)}{=} \|\mathbf{K}^{-1/2}(\mathbf{u}_J - \mathbf{u}_H^i)\|^2 - (\lambda_h^i \|\mathbf{K}^{-1/2}\boldsymbol{\rho}_h^i\|)^2 \\ &\stackrel{(39)}{=} \\ &\stackrel{(38)}{=} \|\mathbf{K}^{-1/2}(\mathbf{u}_J - \mathbf{u}_h^i)\|^2 - \|\mathbf{K}^{-1/2}\boldsymbol{\rho}_H^i\|^2 - (\lambda_h^i \|\mathbf{K}^{-1/2}\boldsymbol{\rho}_h^i\|)^2 \\ &\stackrel{(44)}{=} \|\mathbf{K}^{-1/2}(\mathbf{u}_J - \mathbf{u}_h^i)\|^2 - (\eta_{\text{alg}}^i)^2. \end{aligned}$$

Similarly, for Algorithm 4.2, it holds that

$$\begin{aligned} \|\mathbf{K}^{-1/2}(\mathbf{u}_J - \mathbf{u}_J^{i+1})\|^2 &\stackrel{(31)}{=} \left\| \mathbf{K}^{-1/2} \left(\mathbf{u}_J - \left(\mathbf{u}_J^i + \sum_{j=1}^J \lambda_j^i \boldsymbol{\rho}_j^i \right) \right) \right\|^2 \\ &\stackrel{(13)}{=} \left\| \mathbf{K}^{-1/2} \left(\mathbf{u}_J - \left(\mathbf{u}_J^i + \sum_{j=1}^{J-1} \lambda_j^i \boldsymbol{\rho}_j^i \right) \right) \right\|^2 + 2\lambda_J^i \left(\mathbf{K}^{-1} \left(\mathbf{u}_J^i + \sum_{j=1}^{J-1} \lambda_j^i \boldsymbol{\rho}_j^i \right), \boldsymbol{\rho}_J^i \right) + (\lambda_J^i \|\mathbf{K}^{-1/2}\boldsymbol{\rho}_J^i\|)^2 \\ &\stackrel{(28)}{=} \left\| \mathbf{K}^{-1/2} \left(\mathbf{u}_J - \left(\mathbf{u}_J^i + \sum_{j=1}^{J-1} \lambda_j^i \boldsymbol{\rho}_j^i \right) \right) \right\|^2 - (\lambda_J^i \|\mathbf{K}^{-1/2}\boldsymbol{\rho}_J^i\|)^2 = \dots \\ &= \|\mathbf{K}^{-1/2}(\mathbf{u}_J - \mathbf{u}_J^i)\|^2 - \sum_{j=0}^J (\lambda_j^i \|\mathbf{K}^{-1/2}\boldsymbol{\rho}_j^i\|)^2 \stackrel{(30)}{=} \|\mathbf{K}^{-1/2}(\mathbf{u}_J - \mathbf{u}_J^i)\|^2 - (\eta_{\text{alg}}^i)^2. \end{aligned}$$

The localized writing of the a posteriori estimator (47) (resp. (48)) then follows then from its definition (30) (resp. (44)) and patch-localization (34) (resp. (45)). \square

6.2 Reliability and efficiency of the estimate on the algebraic error

For the a posteriori estimators we introduced, there holds:

Theorem 6.2 (Reliability and efficiency of the algebraic error estimators). *Let either Assumption 3.1 or Assumption 3.2 hold. Let $\mathbf{u}_J^i \in \mathbf{V}_J^f$ be arbitrary. Let η_{alg}^i be constructed from \mathbf{u}_J^i by (30) in Algorithm 4.2 or by (44) in Algorithm 5.1. Then, there holds*

$$\|\mathbf{K}^{-1/2}(\mathbf{u}_J - \mathbf{u}_J^i)\| \geq \eta_{\text{alg}}^i \quad (49)$$

and

$$\beta \|\mathbf{K}^{-1/2}(\mathbf{u}_J - \mathbf{u}_J^i)\| \leq \eta_{\text{alg}}^i, \quad (50)$$

where $0 < \beta \leq 1$ only depends on the mesh-geometry parameters $\kappa_{\mathcal{T}}$, C_{qu} and C_{ref} or C_{qu}^0 and $C_{\text{loc,qu}}$, the diffusion inhomogeneity or anisotropy ratio $\Lambda_{\text{max}}/\Lambda_{\text{min}}$, the domain Ω , at most linearly on the number of mesh levels J , and, if $d = 3$, possibly on the polynomial degree p .

The proof is given in Section 9. Note that the fact that the fully computable estimator η_{alg}^i is a *guaranteed lower bound* on the unknown algebraic error, cf. (49), is an immediate consequence of (46), as the left-hand-side term corresponding to the new algebraic error is nonnegative.

6.3 Error contraction on each solver step

Finally, for the two solvers, there holds:

Theorem 6.3 (Error contraction). *Let either Assumption 3.1 or Assumption 3.2 hold. Let $\mathbf{u}_J^i \in \mathbf{V}_J^f$ be arbitrary. Let $\mathbf{u}_J^{i+1} \in \mathbf{V}_J^f$ be constructed from \mathbf{u}_J^i on step 2 of Algorithm 4.2 or on step 2 of Algorithm 5.1. Then, there holds*

$$\|\mathbf{K}^{-1/2}(\mathbf{u}_J - \mathbf{u}_J^{i+1})\| \leq \alpha \|\mathbf{K}^{-1/2}(\mathbf{u}_J - \mathbf{u}_J^i)\|, \quad (51)$$

where $0 \leq \alpha < 1$ is given by $\alpha = \sqrt{1 - \beta^2}$ with β the constant from (50).

Proof. The (immediate) proof follows from the equivalence of (50) and (51), similarly to [34, Corollary 6.7]. We present it here for completeness. Starting from (51) with $0 \leq \alpha < 1$,

$$\begin{aligned} \|\mathbf{K}^{-1/2}(\mathbf{u}_J - \mathbf{u}_J^{i+1})\|^2 &\leq \alpha^2 \|\mathbf{K}^{-1/2}(\mathbf{u}_J - \mathbf{u}_J^i)\|^2 \\ &\stackrel{(46)}{\iff} \|\mathbf{K}^{-1/2}(\mathbf{u}_J - \mathbf{u}_J^i)\|^2 - (\eta_{\text{alg}}^i)^2 \leq \alpha^2 \|\mathbf{K}^{-1/2}(\mathbf{u}_J - \mathbf{u}_J^i)\|^2 \\ &\iff (1 - \alpha^2) \|\mathbf{K}^{-1/2}(\mathbf{u}_J - \mathbf{u}_J^i)\|^2 \leq (\eta_{\text{alg}}^i)^2. \end{aligned}$$

□

7 Numerical experiments

In this section, we present numerical results for the multigrid solver of Algorithm 4.2 and the domain decomposition method of Algorithm 5.1. Though the implementation aspects are not the main focus of the work, we point out that several options are possible. One can possibly use divergence-free basis functions; for some early contributions on this subject, see, e.g., Thomasset [47], Hecht [22], or Scheichl [41, 42]. This approach may, however, be involved, especially in three space dimensions and for higher polynomial degrees p . We follow here another approach, which consists in using basis

functions of the entire spaces \mathbf{V}_J from (10); these are typically available in finite element software packages. Then, to solve the problems (24) and (26) (or, similarly, (38) and (40)), one uses the fact that they are equivalent to coarse-grid/local saddle-point problems just as (13) is equivalent to (12). Then, no divergence-free basis functions are needed. A special attention needs to be paid when high polynomial degrees p are used, cf., e.g., Kirby [31], Brubeck and Farrell [8] and the references therein.

The experiments are designed to highlight our crucial result stating the p -robustness (proven in Theorems 6.2 and 6.3 in two space dimensions). For this reason, we stop the iterations when the a posteriori algebraic error estimator η_{alg}^i is reduced by the factor 10^5 ; p -robustness is indicated by the number of iterations independent of the polynomial degree p . The experiments are presented for meshes arising from both uniform and local adaptive refinement. For the latter, we employ newest vertex bisection, see e.g. Mitchell [36], Traxler [48], or Stevenson [45], using Dörfler’s bulk-chasing criterion, cf. Dörfler [16], with marking parameter θ_{mark} (specified below) and the true discretization error (instead of a discretization error estimator) for the sake of reproducibility. This criterion reads as: find a set of marked elements $\mathcal{M}_J \subseteq \mathcal{T}_J$ of minimal cardinality that satisfies

$$\theta_{\text{mark}} \|\mathbf{K}^{-1/2}(\mathbf{u} - \mathbf{u}_J)\|^2 \leq \sum_{K \in \mathcal{M}_J} \|\mathbf{K}^{-1/2}(\mathbf{u} - \mathbf{u}_J)\|_K^2.$$

Thus, in the local adaptive case, the obtained mesh hierarchies can be highly graded. Moreover, since we aim to compare the performance of the solver with respect to increasing polynomial degree without other parameters changing, the mesh hierarchy is pre-computed once for each problem using $p = 1$ and re-used in all experiments.

We consider the following test cases (we always take $\mathbf{u} = -\mathbf{K}\nabla\gamma$ and compute f correspondingly):

- **Smooth test case and uniform mesh refinement.** This test is taken from Ewing and Wang [20]:

$$\gamma(x, y) = \cos(\pi x)\cos(\pi y), \quad \Omega = (0, 1)^2. \quad (52)$$

The initial mesh size is taken to be 0.5 and $\mathbf{K} = I$. The refinement is uniform: each existing element is split into four congruent ones by joining the midpoints of its edges.

- **Well wavefront test case and adaptive mesh refinement.** This test case is taken from Mitchell [37]:

$$\gamma(r) = \tan^{-1}(\alpha(r - r_0)), \quad \Omega = (0, 1)^2, \quad (53)$$

where $r = \sqrt{(x - x_c)^2 + (y - y_c)^2}$ and the parameters are $\alpha = 1000$, $x_c = 0.5$, $y_c = 0.5$, $r_0 = 0.01$. The initial mesh size is taken to be 0.5, $\mathbf{K} = I$, and the bulk-chasing parameter for the adaptive refinement is chosen to be $\theta_{\text{mark}} = 0.7$. Figure 3 (left) showcases the mesh obtained after $J = 10$ refinements, zoomed in the vicinity of the “well”.

- **Checkerboard diffusion test case and adaptive mesh refinement.** Consider a singular exact solution written in polar coordinates as

$$\gamma(r, \varphi) = r^\gamma \mu(\varphi), \quad \Omega = (-1, 1)^2, \quad (54)$$

where we follow Kellogg [30] to define $\mu(\varphi)$ and have a regularity parameter $\gamma = 0.0009$ and diffusion contrast 2001405.429972. We illustrate the diffusion coefficient across the domain

in Figure 3 (center). This problem has non-zero Neumann boundary conditions, and the implementation is done by re-adjusting the right-hand side first. The initial mesh size is taken to be 1 and the bulk-chasing parameter for the adaptive refinement is chosen to be $\theta_{\text{mark}} = 0.3$; see Figure 3 (right) for the mesh in the graded hierarchy obtained after $J = 20$ refinements zoomed in the vicinity of the singularity.

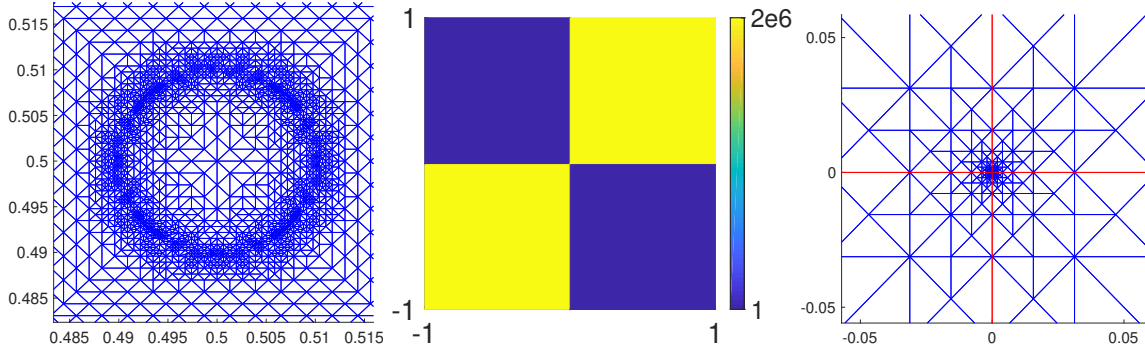


Figure 3: Left: mesh (zoomed in) used for the well wavefront test case (53), obtained after $J = 10$ local adaptive refinements and consisting of 9814 elements. Center: variations of the coefficient $c(x, y)$ for the piecewise constant diffusion tensor $\mathbf{K} = c(x, y) \cdot I$ across the domain for the checkerboard test case (54). Right: mesh (zoomed in) used for the checkerboard test case (54), obtained after $J = 20$ local adaptive refinements and consisting of 1038 elements.

Table 1: Summary of problem sizes in mesh elements and number of degrees of freedom for all the test cases, multigrid and domain decomposition solvers, different polynomial degrees $p = 1, 6$, and mesh hierarchy of J levels.

	Smooth $J = 5$		Wellwavefront $J = 12$		Checkerboard $J = 28$		
	$p = 1$	$p = 6$	$p = 1$	$p = 6$	$p = 1$	$p = 6$	
#DoF (mixed)	130 816	1 318 016	191 486	1 927 051	33 195	334 215	
#DoF (div-free)	82 176	861 056	119 734	1 256 969	20 794	218 134	
$\#\mathcal{T}_J$	16 384	16 384	23 940	23 940	4153	4153	
$\#\mathcal{T}_0$	16	16	16	16	24	24	
MG							
(per patch)	min/max #elements	2/6	2/6	2/10	2/10	2/9	2/9
	min/max #DoF (mixed)	11/41	147/462	11/69	147/770	11/62	147/693
	min/max #DoF (div-free)	6/24	91/294	6/40	91/490	6/36	91/441
DD							
(per subdomain)	min/max #elements	2048/6144	2048/6144	97/22 785	97/22 785	20/3898	20/3898
	min/max #DoF (mixed)	16 256/48 960	164 416/493 920	749/182 203	7714/1 833 923	146/31 156	1561/313 691
	min/max #DoF (div-free)	10 112/30 528	107 072/321 888	458/113 848	4998/1 195 943	86/19 462	1001/204 547

As for the choice of the polynomial degrees per level, recalling (18), any non-decreasing sequence is authorized, allowing in particular for the lowest degree $p = 0$ in the coarse solve, which was tested variedly in [33]. Here, we rather opt for the same polynomial degree p on every level, including the coarsest one, i.e., $p_j = p$ for $0 \leq j \leq J$. The different mesh settings and numbers of unknowns are summarized in Table 1.

In the smooth and well wavefront test cases, using the highest polynomial degree and highest number of mesh refinements leads to saddle-point algebraic systems from (12) with $\sim 2 \cdot 10^6$ degrees of freedom. In the checkerboard test case, due to the point singularity, meshes are aggressively refined towards the origin. In this case, a number of $J = 28$ refinements yields a finest mesh of overall 4153 triangles, but the ratio of the largest to smallest triangle is of order 10^{10} . After this point, numerical computations on further refined meshes start to become numerically unstable in double precision without any specific care.

7.1 Efficiency of the a posteriori error estimator of the algebraic error

Figure 4 gives the effectivity indices of the built-in a posteriori estimators η_{alg}^i of the algebraic error for the multigrid solver (left) and the domain decomposition solver (right) for the different test cases. Recall that η_{alg}^i are respectively given by (30) and (44), whereas the effectivity indices are given by $\eta_{\text{alg}}^i / \|\mathbf{K}^{-1/2}(\mathbf{u}_J - \mathbf{u}_J^i)\|$. From Theorem 6.2, we know that the effectivity indices have to be smaller than or equal to 1 but cannot drop below the constant β , and this uniformly in the polynomial degree p . This p -robustness is confirmed in Figure 4.

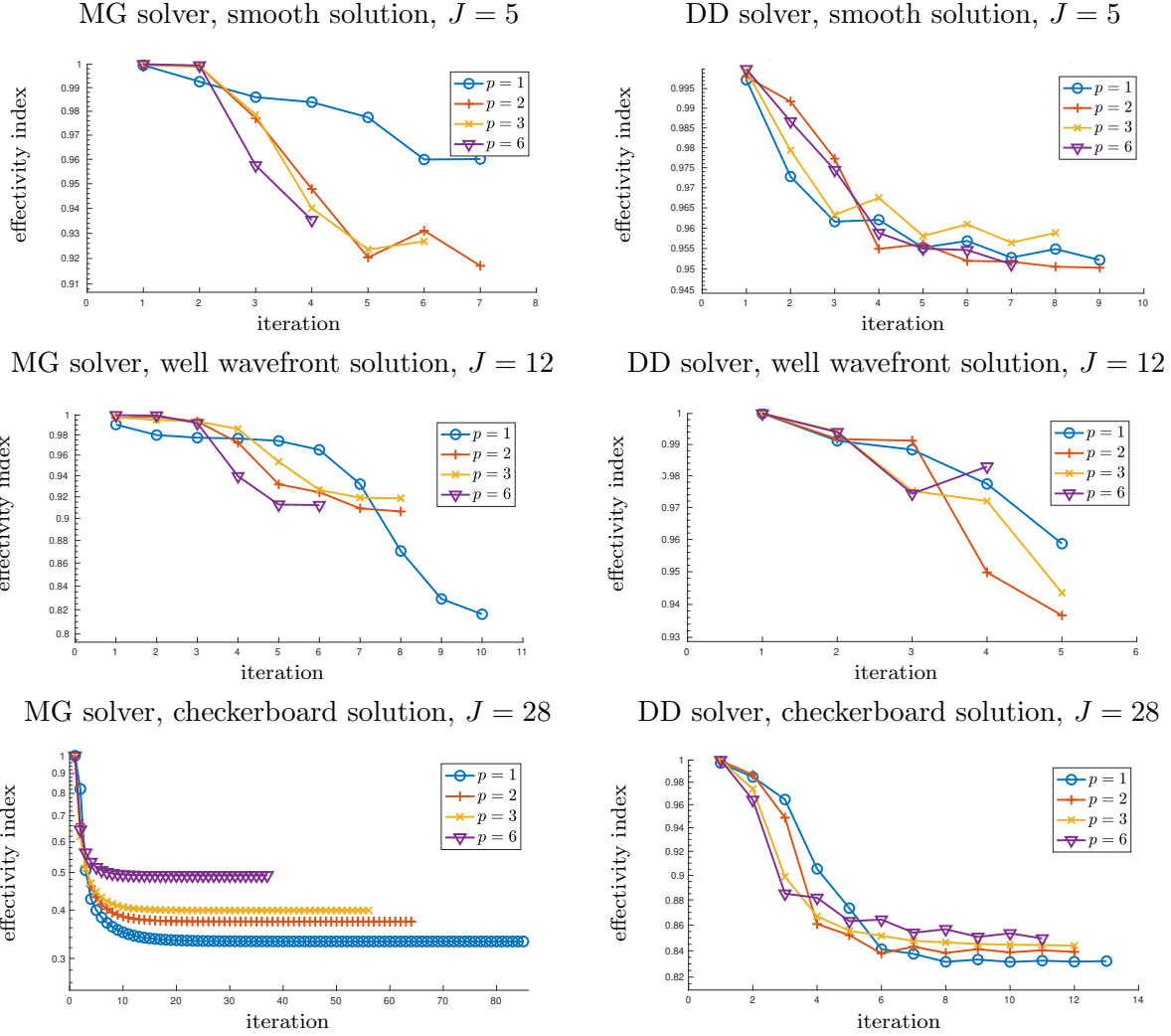


Figure 4: Effectivity index $\eta_{\text{alg}}^i / \|\mathbf{K}^{-1/2}(\mathbf{u}_J - \mathbf{u}_J^i)\|$ of the a posteriori estimator η_{alg}^i for the algebraic error $\|\mathbf{K}^{-1/2}(\mathbf{u}_J - \mathbf{u}_J^i)\|$. Multigrid solver of Algorithm 4.2 (left) and domain decomposition solver of Algorithm 5.1 (right).

7.2 Contraction factors of the solvers

In Figure 5, we report the contraction factors $\|\mathbf{K}^{-1/2}(\mathbf{u}_J - \mathbf{u}_J^{i+1})\| / \|\mathbf{K}^{-1/2}(\mathbf{u}_J - \mathbf{u}_J^i)\|$. From Theorem 6.3, these have to be bounded by the constant α , in particular uniformly in the polynomial

degrees p , which we indeed observe. More precisely, often, even a stronger initial contraction for higher p appears, and then the contraction behaves very similarly for different polynomial degrees throughout the rest of the iterations.

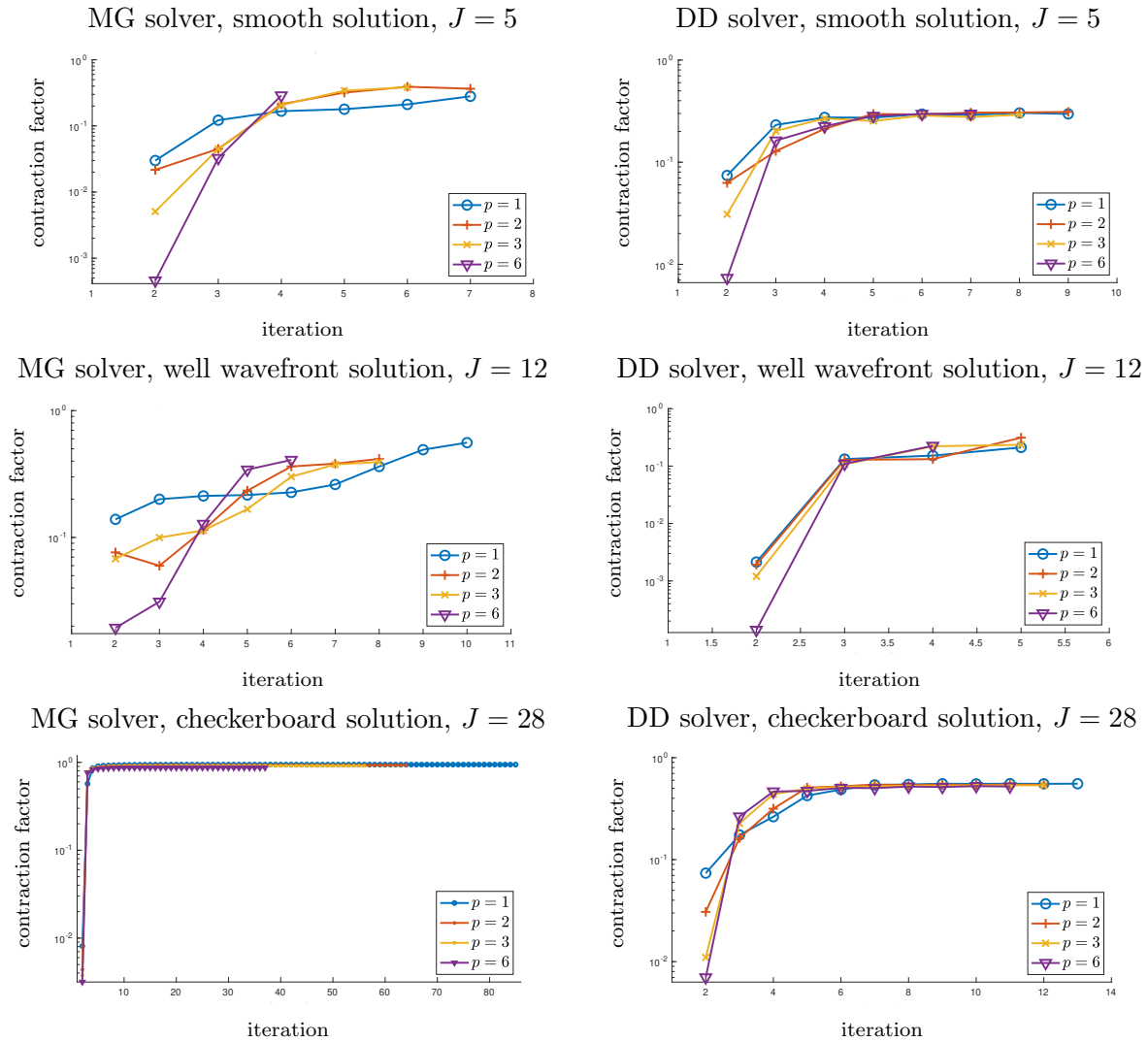


Figure 5: Contraction factors of the solvers given by $\|\mathbf{K}^{-1/2}(\mathbf{u}_J - \mathbf{u}_J^{i+1})\| / \|\mathbf{K}^{-1/2}(\mathbf{u}_J - \mathbf{u}_J^i)\|$. Multigrid solver of Algorithm 4.2 (left) and domain decomposition solver of Algorithm 5.1 (right).

7.3 p -robustness in the number of iterations

Table 2 shows how the p -robustness of the solvers translates to stable (or even decreasing) iteration numbers necessary to reduce the initial a posteriori algebraic error estimator η_{alg}^i by the factor 10^5 . The performance of the multigrid and the domain decomposition solvers appears to be very similar for the smooth solution and uniform refinement case, though the multigrid iteration numbers are slightly smaller overall. Robust numerical performance is also seen in the well wavefront case despite a rougher analytic solution and a larger number of levels in the graded mesh hierarchy. Though we do not refine uniformly here, we still numerically observe no degradation of number of iterations for increasing p with respect to the number of mesh levels J , probably since the solution is regular

enough. It is interesting to note that the domain decomposition method requires slightly smaller iteration numbers compared to the multigrid. An interpretation of this observation can be that as the hierarchy has more levels, the subdomain problems can correct the algebraic error much better due to the size of the local problems compared to the smaller patches used in the multigrid. In the checkerboard case exhibiting a singular solution, the iteration numbers increase with the growth of the number of mesh levels, in at most a linear way, which is in accordance with our main theoretical results; observe, however, that the iteration numbers remain stable (or decrease) with respect to p . This can be seen more easily in the case of the multigrid solver, whereas the increase is very mild for the domain decomposition method; therein, however, much larger subdomain problems have to be solved.

Table 2: Number of iterations needed for the multigrid solver and domain decomposition method to decrease the relative a posteriori estimator of the algebraic error η_{alg}^i by 10^5 , for the test cases (52)–(54) and different polynomial degrees p , number of mesh levels J .

p	Smooth						Wellwavefront						Checkerboard					
	$J = 3$		$J = 4$		$J = 5$		$J = 4$		$J = 8$		$J = 12$		$J = 7$		$J = 14$		$J = 28$	
	MG	DD	MG	DD	MG	DD	MG	DD	MG	DD	MG	DD	MG	DD	MG	DD	MG	DD
1	8	9	8	9	7	9	12	9	10	5	10	5	19	10	37	13	85	13
2	9	9	8	9	7	9	12	7	10	5	8	5	16	11	30	12	64	12
3	8	8	7	8	6	8	10	7	9	5	8	5	15	11	26	11	56	12
6	5	7	4	7	4	7	9	4	8	4	6	4	11	10	18	10	37	11

7.4 Adaptive number of smoothing steps in the multigrid solver

In addition to the efficiency of the estimator η_{alg}^i , Theorem 6.2 together with Theorem 6.1 have yet another important consequence: from (47), η_{alg}^i provides a localized estimation of the algebraic error by levels (and by patches). This is the starting point for an adaptive extension of the multigrid solver following [34, Definition 7.1] with adaptivity parameter $\theta = 0.3$. Instead of employing just one post-smoothing step in Algorithm 4.2 on each level (which, from Theorem 6.3, in contrast to the usual case, is sufficient for overall contraction), an adaptive criterion based on the localized writing of η_{alg}^i discerns whether additional smoothing per level is beneficial. In Table 3, we present a comparison with the non-adaptive variant for the well wavefront test case. The comparison is done in terms of the iteration numbers (#iter.) coinciding with the total number of V-cycles needed to decrease the relative a posteriori estimator of the algebraic error η_{alg}^i by the factor 10^5 , of global synchronizations (#sync.) coinciding with the sum over iterations of the number of smoothing steps and coarse solves, and we moreover display the mean and maximum number of smoothing steps (#smooth.). This approach aims to reduce costs by: 1) lowering the overall number of V-cycles, since intergrid operators for a hierarchy consisting of many levels can become more costly; 2) employing more smoothing steps on lower levels where there are less patches and smoothing is cheaper. As we see from Table 3, the estimator correctly identifies levels requiring more smoothing leading to improved numerical performance by adding one to two more post-smoothing steps only.

7.5 Localization of the algebraic error on levels and patches

While in the previous section we focused on adaptivity based on the levelwise localization of the efficient a posteriori estimator η_{alg}^i , we now investigate numerically the accuracy of the localization both in patches and levels. In Figure 6, we present the patch contributions for different levels of

Table 3: Comparison of Algorithm 4.2 and its version with adaptive number of smoothing steps for the well wavefront test case (53), different polynomial degrees p and number of mesh levels J .

p	$J = 4$			$J = 8$			$J = 12$		
	#iter. adapt/MG	#sync. adapt/MG	#smooth. mean/max	#iter. adapt/MG	#sync. adapt/MG	#smooth. mean/max	#iter. adapt/MG	#sync. adapt/MG	#smooth. mean/max
1	7/12	55/60	1.83/3	7/10	98/90	1.81/2	7/10	133/130	1.71/3
2	6/12	47/60	1.88/3	6/10	83/90	1.84/2	6/8	111/104	1.71/3
3	6/10	44/50	1.76/2	5/9	66/81	1.83/3	5/8	83/104	1.60/3
6	5/9	35/45	1.75/2	5/8	63/72	1.80/3	4/6	56/78	1.44/2

the hierarchy. Since the patches overlap, for ease of visualization, we use the Voronoi dual graph of the triangular mesh connecting the centers of each triangle leading to non-overlapping polygonal representations of the patches. The estimator captures correctly the distribution and the magnitude of the algebraic error throughout the mesh hierarchy. It is interesting to point out that the algebraic error is situated in the regions related to mesh refinement. This is in line with a rich literature on multilevel methods for graded meshes. From the adaptive meshes perspective, smoothing should take place in the patches that were modified in the refinement step, see Section 7.6 below. From the multilevel solver perspective, the local refinement process can also be steered by fully adaptive multigrid method, see, e.g. Růde [40].

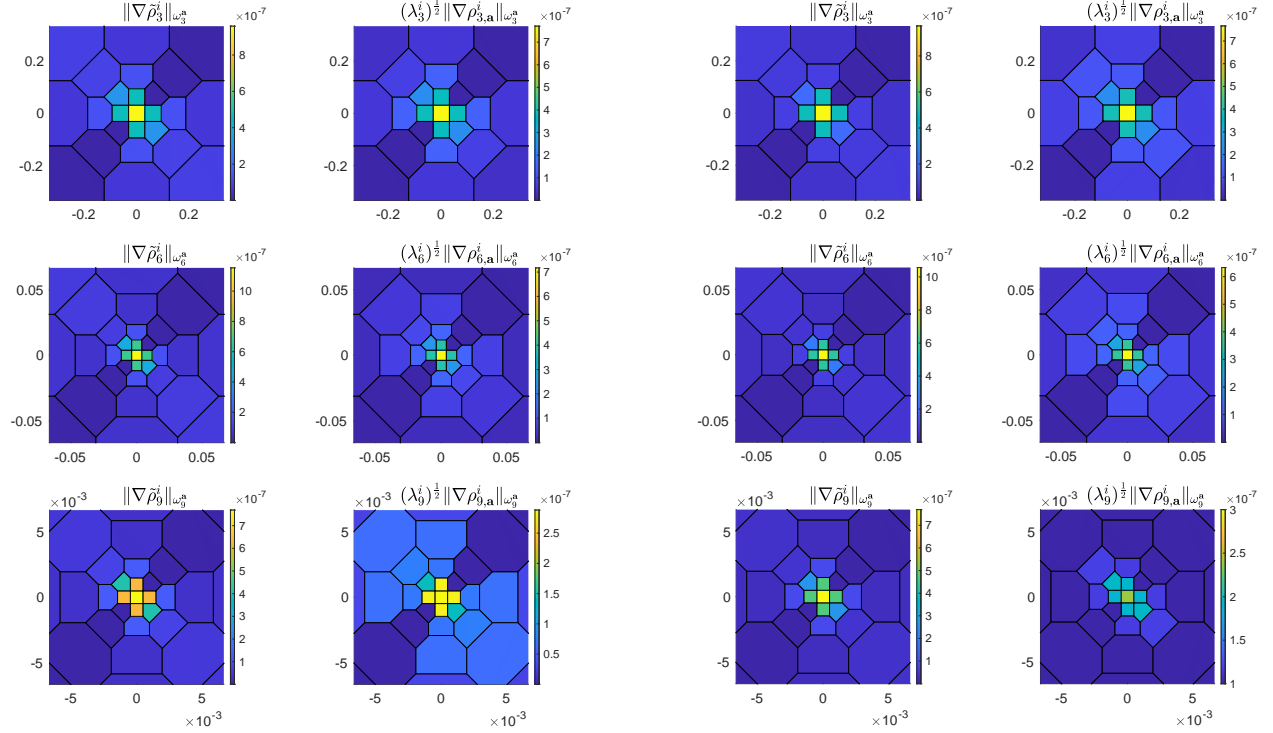


Figure 6: Checkerboard problem, $J = 9$, zoomed towards the origin. Left: patchwise distribution at iteration 7 of the algebraic error (first column) compared to the a posteriori estimator for the algebraic error (second column) for selected levels in the hierarchy and $p = 1$. Right: same experiment for $p = 3$.

7.6 Local smoothing in the multigrid solver

Local solvers as in Chen, Nocketto, and Xu [13], Wu and Zheng [51], or Innerberger et al. [27] allow the solver to tackle only smaller regions in the smoothing phase on each level: this crucially reduces the complexity of the solver, a question that becomes vital when using solvers in combination with adaptive mesh refinement algorithms. Thus, we present here the *local* multigrid solver as a simple modification of our multigrid approach of Algorithm 4.2: instead of smoothing on all patches on each level, we only employ smoothing to patches associated with vertices which are new on the given level with respect to the previous one, as well as existing vertices whose patch has shrunk in size in the mesh refinement step. Recall that each patchwise problem solved via the V-cycle of multigrid provides a local error correction. In comparison, by only smoothing locally relative to the mesh-refinement, the V-cycle of the local multigrid will only give certain – the bulk – of the error corrections of the non-local multigrid. This is to say that the larger error components are localized relative to the mesh-refinement and precisely these components are tackled by local smoothing.

In Table 4, we present a comparison of the original Algorithm 4.2 (MG) with its local modification (locMG). We focus on three aspects. 1) To showcase the localization advantage of locMG through the savings in terms of the number of patch-wise solves, we display the ratio of the average number of patches where smoothing applies in the locMG to all patches (the MG case) (# patches). 2) To present the quality of the error correction, we rely on (46) and (47) to express the computable error decrease of multigrid as

$$\|\mathbf{K}^{-1/2}(\mathbf{u}_J - \mathbf{u}_J^{i+1})\|^2 = \|\mathbf{K}^{-1/2}(\mathbf{u}_J - \mathbf{u}_J^i)\|^2 - \|\mathbf{K}^{-1/2}\boldsymbol{\rho}_0^i\|^2 - \sum_{j=1}^J \lambda_j^i \sum_{\mathbf{a} \in \mathcal{V}_j} \|\mathbf{K}^{-1/2}\boldsymbol{\rho}_{j,\mathbf{a}}^i\|_{\omega_j^{\mathbf{a}}}^2.$$

Similarly, we have for the local version of multigrid

$$\|\mathbf{K}^{-1/2}(\mathbf{u}_J - \mathbf{u}_J^{i+1})\|^2 = \|\mathbf{K}^{-1/2}(\mathbf{u}_J - \mathbf{u}_J^i)\|^2 - \|\mathbf{K}^{-1/2}\boldsymbol{\rho}_0^i\|^2 - \sum_{j=1}^J \lambda_j^i \sum_{\mathbf{a} \in \mathcal{V}_j^+} \|\mathbf{K}^{-1/2}\boldsymbol{\rho}_{j,\mathbf{a}}^i\|_{\omega_j^{\mathbf{a}}}^2,$$

where now the sum is taken only over the new vertices and immediate neighbors $\mathcal{V}_j^+ \subseteq \mathcal{V}_j$. Denoting by i_{MG} and i_{locMG} the iterations of the multigrid and local multigrid, respectively, the average computable decrease in MG is given by

$$\frac{1}{i_{\text{MG}}} \sum_{i=1}^{i_{\text{MG}}} \left(\|\mathbf{K}^{-1/2}\boldsymbol{\rho}_0^i\|^2 + \sum_{j=1}^J \lambda_j^i \sum_{\mathbf{a} \in \mathcal{V}_j} \|\mathbf{K}^{-1/2}\boldsymbol{\rho}_{j,\mathbf{a}}^i\|_{\omega_j^{\mathbf{a}}}^2 \right). \quad (55)$$

Likewise, the average computable decrease in locMG is given by

$$\frac{1}{i_{\text{locMG}}} \sum_{i=1}^{i_{\text{locMG}}} \left(\|\mathbf{K}^{-1/2}\boldsymbol{\rho}_0^i\|^2 + \sum_{j=1}^J \lambda_j^i \sum_{\mathbf{a} \in \mathcal{V}_j^+} \|\mathbf{K}^{-1/2}\boldsymbol{\rho}_{j,\mathbf{a}}^i\|_{\omega_j^{\mathbf{a}}}^2 \right). \quad (56)$$

Thus, we present in Table 4 the ratio of (56) to (55) to compare the error correction (error corr.). 3) To compare a global performance, we show the ratio of the overall number of iterations of locMG to MG (iter.). One can see that the decrease of the algebraic error per iteration is indeed comparable for both methods, while the local multigrid employs a considerably smaller number of patchwise smoothings/local corrections on each level.

Finally, let us mention that the local smoothing region can also be found adaptively in a way disconnected from the local mesh refinement, which is then also applicable in uniformly-refined grids. Such an approach was designed in [35] on the basis of the result corresponding to Theorem 6.1. We do not implement and test it here.

Table 4: Comparison of Algorithm 4.2 and its version with local smoothing for the checkerboard test case (54), different polynomial degrees p and number of mesh levels J .

p	$J = 7$			$J = 14$			$J = 28$		
	# patches locMG/MG	error corr. locMG/MG	iter. locMG/MG	# patches locMG/MG	error corr. locMG/MG	iter. locMG/MG	# patches locMG/MG	error corr. locMG/MG	iter. locMG/MG
1	0.30	0.95	1.05	0.31	0.89	1.05	0.34	0.94	1.04
2	0.30	0.99	1	0.30	0.96	1.03	0.32	0.96	1.01
3	0.30	0.98	1	0.31	0.95	1.04	0.32	0.92	1.03
6	0.30	0.99	1	0.21	0.94	1.06	0.25	0.95	1.03

8 Main theoretical tool: multilevel stable decompositions for divergence-free Raviart–Thomas piecewise polynomials

In our proof of Theorem 6.2 (and thus of Theorem 6.3), which we present in Section 9 below, a crucial ingredient is the existence of a suitable stable decomposition of the space \mathbf{V}_J^0 defined in (20), i.e., the space of divergence-free Raviart–Thomas $\mathbf{H}_0(\text{div}; \Omega)$ -conforming piecewise polynomials. We achieve this in Proposition 8.5 at the end of this section, following some intermediate results that are of their own interest and are presented below in the form of lemmas.

8.1 Multilevel p -robustly stable decomposition for Lagrange piecewise polynomials

First, we recall for the reader’s convenience the multilevel p -robustly stable decomposition for any function of the stream-function space $S_J := \mathbb{P}_{p+1}(\mathcal{T}_J) \cap H_0^1(\Omega)$, $p \geq 0$, in the $H_0^1(\Omega)$ -norm $\|\nabla \cdot\|$. This result has been shown in [33, Proposition 7.6] by combining the results of Schöberl et al. [43] and Xu, Chen, and Nochetto [52].

Lemma 8.1 (Multilevel p -robustly stable decomposition of S_J). *Under either Assumption 3.1 or Assumption 3.2, for any $v_J \in S_J$, there exists a decomposition*

$$v_J = v_0 + \sum_{j=1}^J \sum_{\mathbf{a} \in \mathcal{V}_j} v_{j,\mathbf{a}}, \quad (57a)$$

with $v_0 \in S_0^1 := \mathbb{P}_1(\mathcal{T}_0) \cap H_0^1(\Omega)$ (global coarse-grid lowest-order component) and $v_{j,\mathbf{a}} \in S_j^\mathbf{a} := \mathbb{P}_{p+1}(\mathcal{T}_j) \cap H_0^1(\omega_j^\mathbf{a})$, $1 \leq j \leq J$, $\mathbf{a} \in \mathcal{V}_j$, (levelwise and local patchwise high-order components) stable as

$$\|\nabla v_0\|^2 + \sum_{j=1}^J \sum_{\mathbf{a} \in \mathcal{V}_j} \|\nabla v_{j,\mathbf{a}}\|_{\omega_j^\mathbf{a}}^2 \leq C_{\text{SD}}^2 \|\nabla v_J\|^2, \quad (57b)$$

with C_{SD} depending on the mesh shape regularity parameter $\kappa_{\mathcal{T}}$ and additionally on the parameters C_{qu} and C_{ref} when Assumption 3.1 is satisfied or on the parameters C_{qu}^0 and $C_{\text{loc,qu}}$ when Assumption 3.2 is satisfied. In particular, C_{SD} is independent of the number of mesh levels J and of the polynomial degree p .

8.2 Stable discrete potential for the lowest-order divergence-free Raviart–Thomas piecewise polynomials in three space dimensions

In order to present the following result, we introduce the elementwise Nédélec spaces with $d = 3$, see Nédélec [38], by $\mathbf{N}_p(K) := [\mathbb{P}_p(K)]^3 + \mathbf{x} \times \mathbb{P}_p(K)^3$ for any element $K \in \mathcal{T}_J$. Similarly to (6)

and (10), let

$$\mathbf{X} := \mathbf{H}_0(\mathbf{curl}; \Omega) := \{\mathbf{v} \in \mathbf{H}(\mathbf{curl}; \Omega), \mathbf{v} \times \mathbf{n} = 0 \text{ on } \partial\Omega \text{ in appropriate sense}\} \quad (58)$$

and

$$\mathbf{N}_{J,0} := \{\mathbf{v}_J \in \mathbf{X}, \mathbf{v}_J|_K \in \mathbf{N}_0(K) \forall K \in \mathcal{T}_J\}. \quad (59)$$

Lemma 8.2 (Stable discrete potential in three space dimensions). *Let $d = 3$. For any $\mathbf{v}_J \in \mathbf{V}_J^0 \cap \mathbf{RT}_0(\mathcal{T}_J)$, there is a stable discrete vector potential $\boldsymbol{\xi}_J \in \mathbf{N}_{J,0}$ such that*

$$\mathbf{v}_J = \nabla \times \boldsymbol{\xi}_J \quad \text{and} \quad \|\boldsymbol{\xi}_J\| \leq C_{\text{pot}} \|\mathbf{v}_J\|, \quad (60)$$

where the constant C_{pot} only depends on the mesh shape regularity parameter $\kappa_{\mathcal{T}}$ and the domain Ω .

Proof. This result can be obtained as in, e.g., by Hiptmair and Xu [26, Section 4]. For completeness, we present a direct proof. Consider the following discrete minimization problem

$$\boldsymbol{\xi}_J := \arg \min_{\substack{\boldsymbol{\zeta}_J \in \mathbf{N}_{J,0} \\ \nabla \times \boldsymbol{\zeta}_J = \mathbf{v}_J}} \|\boldsymbol{\zeta}_J\|. \quad (61)$$

This problem is well posed since the datum \mathbf{v}_J is a divergence-free Raviart–Thomas $\mathbf{H}_0(\text{div}; \Omega)$ -conforming piecewise polynomial and since Ω is homotopic to a ball. We also define its counterpart on the continuous level,

$$\boldsymbol{\xi} := \arg \min_{\substack{\boldsymbol{\zeta} \in \mathbf{X} \\ \nabla \times \boldsymbol{\zeta} = \mathbf{v}_J}} \|\boldsymbol{\zeta}\|. \quad (62)$$

We now employ the commuting projector $\mathbf{P}_J^{0,\text{curl}}$ of Chaumont-Frelet and Vohralík [11, Definition 3.3]. Note that $\mathbf{P}_J^{0,\text{curl}}(\boldsymbol{\xi}) \in \mathbf{N}_{J,0}$ with $\nabla \times (\mathbf{P}_J^{0,\text{curl}}(\boldsymbol{\xi})) = \nabla \times \boldsymbol{\xi} = \mathbf{v}_J$, since $\nabla \times \boldsymbol{\xi} = \mathbf{v}_J \in \mathbf{V}_J^0 \cap \mathbf{RT}_0(\mathcal{T}_J)$. Consequently, the minimization property (61) together with [11, Theorem 3.6, (3.18)] give

$$\|\boldsymbol{\xi}_J\| \leq \|\mathbf{P}_J^{0,\text{curl}}(\boldsymbol{\xi})\| \leq C_{\kappa_{\mathcal{T}}} \|\boldsymbol{\xi}\| \quad (63)$$

for $C_{\kappa_{\mathcal{T}}} > 0$ only depending on the shape regularity parameter $\kappa_{\mathcal{T}}$, since all discrete functions considered here are of lowest order.

Note now that (62) can be equivalently written as searching for the solution $(\boldsymbol{\xi}, \mathbf{z})$, with $\boldsymbol{\xi} \in \mathbf{X}$ and $\mathbf{z} \in \mathbf{V}^0$, to the problem

$$(\boldsymbol{\xi}, \boldsymbol{\zeta}) + (\mathbf{z}, \nabla \times \boldsymbol{\zeta}) = 0 \quad \forall \boldsymbol{\zeta} \in \mathbf{X}, \quad (64a)$$

$$(\nabla \times \boldsymbol{\xi}, \mathbf{w}) = (\mathbf{v}_J, \mathbf{w}) \quad \forall \mathbf{w} \in \mathbf{V}^0. \quad (64b)$$

In particular, note that $\mathbf{z} \in \mathbf{V}^0$, and from (64a) it satisfies

$$(\mathbf{z}, \nabla \times \boldsymbol{\zeta}) = -(\boldsymbol{\xi}, \boldsymbol{\zeta}) \quad \forall \boldsymbol{\zeta} \in \mathbf{X}. \quad (65)$$

This means that \mathbf{z} belongs to $\mathbf{H}(\mathbf{curl}; \Omega)$ and weakly satisfies $\nabla \times \mathbf{z} = \boldsymbol{\xi}$. By Poincaré–Friedrichs–Weber’s inequality, see e.g. Weber [49] or Boffi, Brezzi, and Fortin [3, Section 11.1.2], one then obtains

$$\|\mathbf{z}\| \leq C_{\text{PFW}h_{\Omega}} \|\nabla \times \mathbf{z}\| = C_{\text{PFW}h_{\Omega}} \|\boldsymbol{\xi}\|, \quad (66)$$

where C_{PFW} is a generic constant of order of unity and h_Ω denotes the diameter of the domain Ω .

To prove the stability in (60) it is now sufficient to take $\boldsymbol{\zeta} = \boldsymbol{\xi}$ and $\boldsymbol{w} = \boldsymbol{z}$ as test functions in (64) and subtract the two resulting subequations, yielding

$$\|\boldsymbol{\xi}\|^2 = -(\boldsymbol{v}_J, \boldsymbol{z}) \leq \|\boldsymbol{v}_J\| \|\boldsymbol{z}\| \stackrel{(66)}{\leq} C_{\text{PFW}} h_\Omega \|\boldsymbol{v}_J\| \|\boldsymbol{\xi}\|. \quad (67)$$

Finally, combining with (63),

$$\|\boldsymbol{\xi}_J\| \stackrel{(63)}{\leq} C_{\kappa_{\mathcal{T}}} \|\boldsymbol{\xi}\| \stackrel{(67)}{\leq} \underbrace{C_{\kappa_{\mathcal{T}}} C_{\text{PFW}} h_\Omega}_{C_{\text{pot}}} \|\boldsymbol{v}_J\|.$$

□

8.3 One-level stable decomposition for high-order divergence-free Raviart–Thomas piecewise polynomials in three space dimensions

We now tackle a stable decomposition of \mathbf{V}_J^0 from (20) on the finest level \mathcal{T}_J , employing local divergence-free spaces $\mathbf{V}_J^{\mathbf{a},0}$ from (23).

Lemma 8.3 (One-level high-order stable decomposition of \mathbf{V}_J^0 in three space dimensions). *Let either Assumption 3.1 or Assumption 3.2 hold. Assume moreover that $d = 3$. For any $\boldsymbol{v}_J \in \mathbf{V}_J^0$, there exist $\boldsymbol{\delta}_{J,0} \in \mathbf{V}_J^0 \cap \mathbf{RT}_0(\mathcal{T}_J)$ (global lowest-order component) and $\boldsymbol{\delta}_{J,\mathbf{a}} \in \mathbf{V}_J^{\mathbf{a},0}$, $\mathbf{a} \in \mathcal{V}_J$, (local patchwise high-order components) such that*

$$\boldsymbol{v}_J = \boldsymbol{\delta}_{J,0} + \sum_{\mathbf{a} \in \mathcal{V}_J} \boldsymbol{\delta}_{J,\mathbf{a}} \quad (68a)$$

is stable as

$$\|\mathbf{K}^{-1/2} \boldsymbol{\delta}_{J,0}\|^2 + \sum_{\mathbf{a} \in \mathcal{V}_J} \|\mathbf{K}^{-1/2} \boldsymbol{\delta}_{J,\mathbf{a}}\|_{\omega_{\mathbf{a}}}^2 \leq C_{\text{OL}}^2 \|\mathbf{K}^{-1/2} \boldsymbol{v}_J\|^2, \quad (68b)$$

where the constant C_{OL} only depends on the mesh-geometry parameters $\kappa_{\mathcal{T}}$, C_{qu} and C_{ref} or C_{qu}^0 and $C_{\text{loc,qu}}$, the diffusion inhomogeneity or anisotropy ratio $\Lambda_{\text{max}}/\Lambda_{\text{min}}$, and possibly on the polynomial degree p .

Proof. The proof is presented in six steps and consists in initially introducing a lowest-order stable component of \boldsymbol{v}_J and constructing afterwards a local stable decomposition of the remaining high-order components. The latter decomposition relies on techniques following Chaumont-Frelet and Vohralík [10, Theorem B.1].

First, for ease of notation, we introduce the Raviart–Thomas interpolant of order $q \geq 0$ given elementwise as follows: for any $K \in \mathcal{T}_J$ and any $\boldsymbol{w} \in [C^1(K)]^3$, construct $\mathbf{I}_{K,q}^{\mathbf{RT}}(\boldsymbol{w}) \in \mathbf{RT}_q(K)$ such that

$$(\mathbf{I}_{K,q}^{\mathbf{RT}}(\boldsymbol{w}) \cdot \boldsymbol{n}_K, r_J)_F = (\boldsymbol{w} \cdot \boldsymbol{n}_K, r_J)_F \quad \forall r_J \in \mathbb{P}_q(F), \forall F \in \mathcal{F}_K, \quad (69a)$$

$$(\mathbf{I}_{K,q}^{\mathbf{RT}}(\boldsymbol{w}), \boldsymbol{r}_J)_K = (\boldsymbol{w}, \boldsymbol{r}_J)_K \quad \forall \boldsymbol{r}_J \in [\mathbb{P}_{q-1}(K)]^3, \quad (69b)$$

where \mathcal{F}_K denotes the faces of the simplex K . Moreover, we denote by $\Pi_{K,q}$ the elementwise $L^2(K)$ -orthogonal projection onto $\mathbb{P}_q(K)$ for all $K \in \mathcal{T}_J$, $q > 0$. Similarly, let Π_q denote the $L^2(\Omega)$ -orthogonal projection onto $\mathbb{P}_q(\mathcal{T}_J) := \{\boldsymbol{w}_J \in L^2(\Omega), \boldsymbol{w}_J|_K \in \mathbb{P}_q(K) \quad \forall K \in \mathcal{T}_J\}$, $q > 0$.

Finally, let the elementwise $[L^2(K)]^d$ -orthogonal projection $\mathbf{\Pi}_{K,q}$ be given componentwise by $\Pi_{K,q}$, for all $K \in \mathcal{T}_J$ and $q > 0$. The following elementwise commuting property holds for $\mathbf{I}_{K,q}^{RT}$: for any $\mathbf{w} \in [C^1(K)]^3$

$$\nabla \cdot \mathbf{I}_{K,q}^{RT}(\mathbf{w}) = \Pi_{K,q}(\nabla \cdot \mathbf{w}). \quad (70)$$

Step 1: Construction of the divergence-free lowest-order component. Let $\psi_{J,\mathbf{a}}$ denote the piecewise affine hat function that takes value one in vertex $\mathbf{a} \in \mathcal{V}_J$ and zero in all other vertices of \mathcal{V}_J . Define, for all vertices $\mathbf{a} \in \mathcal{V}_J$ and all elements $K \in \mathcal{T}_J$ sharing \mathbf{a} ,

$$\delta_{J,0}^{\mathbf{a}}|_K := \mathbf{I}_{K,0}^{RT}((\psi_{J,\mathbf{a}}\mathbf{v}_J)|_K), \quad (71a)$$

$$\delta_{J,0} := \sum_{\mathbf{a} \in \mathcal{V}_J} \delta_{J,0}^{\mathbf{a}}. \quad (71b)$$

Since $\mathbf{v}_J \in \mathbf{V}_J^0$, i.e. $\mathbf{v}_J \in \mathbf{RT}_p(\mathcal{T}_J) \cap \mathbf{H}_0(\text{div}; \Omega)$ and $\nabla \cdot \mathbf{v}_J = 0$, there holds $\delta_{J,0}^{\mathbf{a}} \in \mathbf{RT}_0(\mathcal{T}_J^{\mathbf{a}}) \cap \mathbf{H}_0(\text{div}; \omega_J^{\mathbf{a}})$, leading to $\delta_{J,0} \in \mathbf{RT}_0(\mathcal{T}_J) \cap \mathbf{H}_0(\text{div}; \Omega)$. Next, we use the commuting property (70), the partition of unity for the hat functions $\sum_{\mathbf{a} \in \mathcal{V}_J} \psi_{J,\mathbf{a}} = 1$, and $\nabla \cdot \mathbf{v}_J = 0$, to obtain

$$\begin{aligned} \nabla \cdot \delta_{J,0} &\stackrel{(71b)}{=} \sum_{\mathbf{a} \in \mathcal{V}_J} \nabla \cdot \delta_{J,0}^{\mathbf{a}} \stackrel{(71a)}{=} \sum_{\mathbf{a} \in \mathcal{V}_J} \sum_{K \in \mathcal{T}_J^{\mathbf{a}}} \nabla \cdot \mathbf{I}_{K,0}^{RT}((\psi_{J,\mathbf{a}}\mathbf{v}_J)|_K) \stackrel{(70)}{=} \sum_{\mathbf{a} \in \mathcal{V}_J} \sum_{K \in \mathcal{T}_J^{\mathbf{a}}} \Pi_{K,0}(\nabla \cdot (\psi_{J,\mathbf{a}}\mathbf{v}_J)|_K) \\ &= \sum_{\mathbf{a} \in \mathcal{V}_J} \sum_{K \in \mathcal{T}_J^{\mathbf{a}}} \Pi_{K,0}(\nabla \psi_{J,\mathbf{a}} \cdot \mathbf{v}_J + \psi_{J,\mathbf{a}} \nabla \cdot \mathbf{v}_J)|_K = \Pi_0(\nabla \mathbf{1} \cdot \mathbf{v}_J + \nabla \cdot \mathbf{v}_J) = 0. \end{aligned} \quad (72)$$

This means that $\delta_{J,0} \in \mathbf{V}_J^0 \cap \mathbf{RT}_0(\mathcal{T}_J)$ as requested.

Step 2: Stability of the divergence-free lowest-order component. The stability of the lowest-order divergence-free component with respect to \mathbf{v}_J follows as

$$\begin{aligned} \|\delta_{J,0}\|_K^2 &\stackrel{(71b)}{=} \left\| \sum_{\mathbf{a} \in \mathcal{V}_K} \delta_{J,0}^{\mathbf{a}} \right\|_K^2 \leq (d+1) \sum_{\mathbf{a} \in \mathcal{V}_K} \|\delta_{J,0}^{\mathbf{a}}\|_K^2 \leq (d+1) \sum_{\mathbf{a} \in \mathcal{V}_K} \|\delta_{J,0}^{\mathbf{a}}\|_{\omega_J^{\mathbf{a}}}^2 \\ &\stackrel{(71a)}{=} (d+1) \sum_{\mathbf{a} \in \mathcal{V}_K} \sum_{K \in \mathcal{T}_J^{\mathbf{a}}} \|\mathbf{I}_{K,0}^{RT}((\psi_{J,\mathbf{a}}\mathbf{v}_J)|_K)\|_K^2 \leq C_0(d+1) \sum_{\mathbf{a} \in \mathcal{V}_K} \|\psi_{J,\mathbf{a}}\mathbf{v}_J\|_{\omega_J^{\mathbf{a}}}^2 \\ &\leq C_0(d+1) \sum_{\mathbf{a} \in \mathcal{V}_K} \|\psi_{J,\mathbf{a}}\|_{\infty, \omega_J^{\mathbf{a}}}^2 \|\mathbf{v}_J\|_{\omega_J^{\mathbf{a}}}^2 = C_0(d+1) \sum_{\mathbf{a} \in \mathcal{V}_K} \|\mathbf{v}_J\|_{\omega_J^{\mathbf{a}}}^2, \end{aligned} \quad (73)$$

where the constant $C_0 > 0$ arises from the stability of the elementwise Raviart–Thomas interpolant defined in (69), see e.g., [17, Chapter 16]. Summing over the elements yields the desired bound

$$\|\delta_{J,0}\|^2 = \sum_{K \in \mathcal{T}_J} \|\delta_{J,0}\|_K^2 \stackrel{(73)}{\leq} \sum_{K \in \mathcal{T}_J} C_0(d+1) \sum_{\mathbf{a} \in \mathcal{V}_K} \|\mathbf{v}_J\|_{\omega_J^{\mathbf{a}}}^2 \leq C_{\kappa_{\mathcal{T}}} C_0(d+1) \|\mathbf{v}_J\|^2, \quad (74)$$

where $C_{\kappa_{\mathcal{T}}} > 0$ only depends on the mesh shape-regularity parameter $\kappa_{\mathcal{T}}$.

Step 3: Construction of the high-order divergence-free local components. In the following steps we pursue the approach of Chaumont-Frelet and Vohralík [10, Theorem B.1] to construct local stable high-order contributions of \mathbf{v}_J . Consider the following elementwise construction for all vertices $\mathbf{a} \in \mathcal{V}_J$ and all elements $K \in \mathcal{T}_J$ sharing \mathbf{a} :

$$\begin{aligned} \delta_{J,\mathbf{a}}|_K := & \arg \min_{\substack{\mathbf{w}_J \in \mathbf{RT}_p(K) \\ \nabla \cdot \mathbf{w}_J = 0}} \left\| (\mathbf{I}_{K,p}^{RT}((\psi_{J,\mathbf{a}}\mathbf{v}_J)|_K) - \delta_{J,0}^{\mathbf{a}}) - \mathbf{w}_J \right\|_K. \\ & \mathbf{w}_J \cdot \mathbf{n} = (\mathbf{I}_{K,p}^{RT}((\psi_{J,\mathbf{a}}\mathbf{v}_J)|_K) - \delta_{J,0}^{\mathbf{a}}) \cdot \mathbf{n} \text{ on } \partial K \end{aligned} \quad (75)$$

The well-posedness of such a problem is equivalent to the Neumann compatibility condition $((\mathbf{I}_{K,p}^{RT}((\psi_{J,\mathbf{a}}\mathbf{v}_J)|_K) - \boldsymbol{\delta}_{J,0}^{\mathbf{a}}) \cdot \mathbf{n}, 1)_{\partial K} = 0$ being satisfied, see e.g. Boffi, Brezzi, and Fortin [3]. This condition is indeed satisfied, thanks to the definition of $\boldsymbol{\delta}_{J,0}$ and the Raviart–Thomas interpolation using that $1 \in \mathbb{P}_0(\partial K)$

$$\begin{aligned} ((\mathbf{I}_{K,p}^{RT}((\psi_{J,\mathbf{a}}\mathbf{v}_J)|_K) - \boldsymbol{\delta}_{J,0}^{\mathbf{a}}) \cdot \mathbf{n}, 1)_{\partial K} &\stackrel{(71a)}{=} ((\mathbf{I}_{K,p}^{RT}((\psi_{J,\mathbf{a}}\mathbf{v}_J)|_K) - (\mathbf{I}_{K,0}^{RT}((\psi_{J,\mathbf{a}}\mathbf{v}_J)|_K)) \cdot \mathbf{n}, 1)_{\partial K} \\ &\stackrel{(69a)}{=} ((\psi_{J,\mathbf{a}}\mathbf{v}_J)|_K \cdot \mathbf{n}, 1)_{\partial K} - ((\psi_{J,\mathbf{a}}\mathbf{v}_J)|_K \cdot \mathbf{n}, 1)_{\partial K} = 0. \end{aligned}$$

By construction of the normal components and the divergence constraint in (75), the local high-order contributions belong indeed to the local spaces $\mathbf{V}_J^{\mathbf{a},0}$ defined by (23) for all $\mathbf{a} \in \mathcal{V}_J$, i.e.,

$$\boldsymbol{\delta}_{J,\mathbf{a}} \in \mathbf{RT}_p(\mathcal{T}_J^{\mathbf{a}}) \cap \mathbf{H}_0(\text{div}; \omega_J^{\mathbf{a}}) \quad \text{and} \quad \nabla \cdot \boldsymbol{\delta}_{J,\mathbf{a}} = 0.$$

Step 4: Stability of the high-order divergence-free local components. To show stability of the high-order divergence-free local components with respect to \mathbf{v}_J , we first introduce, for all $\mathbf{a} \in \mathcal{V}_J$ and all $K \in \mathcal{T}_J^{\mathbf{a}}$, auxiliary elementwise constructions

$$\begin{aligned} \widehat{\boldsymbol{\delta}}_{J,\mathbf{a}}|_K := & \arg \min_{\substack{\mathbf{w}_J \in \mathbf{RT}_p(K) \\ \nabla \cdot \mathbf{w}_J = \nabla \cdot (\mathbf{I}_{K,p}^{RT}((\psi_{J,\mathbf{a}}\mathbf{v}_J)|_K) - \boldsymbol{\delta}_{J,0}^{\mathbf{a}}) \\ \mathbf{w}_J \cdot \mathbf{n} = 0 \text{ on } \partial K}} \|\mathbf{w}_J\|_K. \end{aligned} \quad (76)$$

These problems are also well-posed as the Neumann compatibility condition holds,

$$\begin{aligned} (\nabla \cdot (\mathbf{I}_{K,p}^{RT}((\psi_{J,\mathbf{a}}\mathbf{v}_J)|_K) - \boldsymbol{\delta}_{J,0}^{\mathbf{a}}), 1)_K &\stackrel{(71a)}{=} (\nabla \cdot (\mathbf{I}_{K,p}^{RT}((\psi_{J,\mathbf{a}}\mathbf{v}_J)|_K) - \mathbf{I}_{K,0}^{RT}((\psi_{J,\mathbf{a}}\mathbf{v}_J)|_K)), 1)_K \\ &\stackrel{(70)}{=} (\Pi_{K,p}(\nabla \cdot (\psi_{J,\mathbf{a}}\mathbf{v}_J)|_K) - \Pi_{K,0}(\nabla \cdot (\psi_{J,\mathbf{a}}\mathbf{v}_J)|_K), 1)_K = 0, \end{aligned} \quad (77)$$

where we have used the definition of the elementwise $L^2(K)$ -orthogonal projection. By construction, problems (75) and (76) lead to

$$\widehat{\boldsymbol{\delta}}_{J,\mathbf{a}}|_K = \mathbf{I}_{K,p}^{RT}((\psi_{J,\mathbf{a}}\mathbf{v}_J)|_K) - \boldsymbol{\delta}_{J,0}^{\mathbf{a}}|_K - \boldsymbol{\delta}_{J,\mathbf{a}}|_K. \quad (78)$$

Following Ern and Vohralík [18, Lemma A.3], one obtains for $C_{\text{stab}} > 0$ only depending on mesh shape regularity the stability result

$$\begin{aligned} \min_{\substack{\mathbf{w}_J \in \mathbf{RT}_p(K) \\ \nabla \cdot \mathbf{w}_J = \nabla \cdot (\mathbf{I}_{K,p}^{RT}((\psi_{J,\mathbf{a}}\mathbf{v}_J)|_K) - \boldsymbol{\delta}_{J,0}^{\mathbf{a}}) \\ \mathbf{w}_J \cdot \mathbf{n} = 0 \text{ on } \partial K}} \|\mathbf{w}_J\|_K \leq C_{\text{stab}} \min_{\substack{\mathbf{v} \in \mathbf{H}(\text{div}, K) \\ \nabla \cdot \mathbf{v} = \nabla \cdot (\mathbf{I}_{K,p}^{RT}((\psi_{J,\mathbf{a}}\mathbf{v}_J)|_K) - \boldsymbol{\delta}_{J,0}^{\mathbf{a}}) \\ \mathbf{v} \cdot \mathbf{n} = 0 \text{ on } \partial K}} \|\mathbf{v}\|_K. \end{aligned} \quad (79)$$

Thus, we have

$$\begin{aligned} \|\boldsymbol{\delta}_{J,\mathbf{a}} - (\mathbf{I}_{K,p}^{RT}((\psi_{J,\mathbf{a}}\mathbf{v}_J)|_K) - \boldsymbol{\delta}_{J,0}^{\mathbf{a}})\|_K &\stackrel{(78)}{=} \|\widehat{\boldsymbol{\delta}}_{J,\mathbf{a}}\|_K \stackrel{(76)}{=} \min_{\substack{\mathbf{w}_J \in \mathbf{RT}_p(K) \\ \nabla \cdot \mathbf{w}_J = \nabla \cdot (\mathbf{I}_{K,p}^{RT}((\psi_{J,\mathbf{a}}\mathbf{v}_J)|_K) - \boldsymbol{\delta}_{J,0}^{\mathbf{a}}) \\ \mathbf{w}_J \cdot \mathbf{n} = 0 \text{ on } \partial K}} \|\mathbf{w}_J\|_K \\ &\stackrel{(79)}{\leq} C_{\text{stab}} \min_{\substack{\mathbf{v} \in \mathbf{H}(\text{div}, K) \\ \nabla \cdot \mathbf{v} = \nabla \cdot (\mathbf{I}_{K,p}^{RT}((\psi_{J,\mathbf{a}}\mathbf{v}_J)|_K) - \boldsymbol{\delta}_{J,0}^{\mathbf{a}}) \\ \mathbf{v} \cdot \mathbf{n} = 0 \text{ on } \partial K}} \|\mathbf{v}\|_K \\ &= C_{\text{stab}} \|\nabla \zeta_K\|_K, \end{aligned}$$

where $\zeta_K \in H_*^1(K) := \{v \in H^1(K), (v, 1)_K = 0\}$ solves the equivalent primal problem

$$(\nabla \zeta_K, \nabla v)_K = (\nabla \cdot (\mathbf{I}_{K,p}^{RT}((\psi_{J,\mathbf{a}} \mathbf{v}_J)|_K) - \boldsymbol{\delta}_{J,0}^{\mathbf{a}}), v)_K \quad \forall v \in H_*^1(K). \quad (80)$$

Next, continuing (77), we see that

$$\begin{aligned} \nabla \cdot (\mathbf{I}_{K,p}^{RT}((\psi_{J,\mathbf{a}} \mathbf{v}_J)|_K) - \boldsymbol{\delta}_{J,0}^{\mathbf{a}}) &= \Pi_{K,p}(\nabla \cdot (\psi_{J,\mathbf{a}} \mathbf{v}_J)|_K) - \Pi_{K,0}(\nabla \cdot (\psi_{J,\mathbf{a}} \mathbf{v}_J)|_K) \\ &= \Pi_{K,p}((\nabla \psi_{J,\mathbf{a}} \cdot \mathbf{v}_J + 0)|_K) - \Pi_{K,0}((\nabla \psi_{J,\mathbf{a}} \cdot \mathbf{v}_J + 0)|_K) \\ &= \nabla \psi_{J,\mathbf{a}}|_K \cdot (\mathbf{v}_J|_K - \mathbf{\Pi}_{K,0}(\mathbf{v}_J|_K)), \end{aligned} \quad (81)$$

since \mathbf{v}_J is divergence-free and thus actually p -degree polynomial in each component, see, e.g., [3, Corollary 2.3.1]. Consequently, we can pursue our main estimate using the Cauchy–Schwarz and the Poincaré inequality

$$\begin{aligned} \|\boldsymbol{\delta}_{J,\mathbf{a}} - (\mathbf{I}_{K,p}^{RT}((\psi_{J,\mathbf{a}} \mathbf{v}_J)|_K) - \boldsymbol{\delta}_{J,0}^{\mathbf{a}})\|_K &\lesssim \|\nabla \zeta_K\|_K = \max_{\substack{v \in H_*^1(K) \\ \|\nabla v\|_K=1}} (\nabla \zeta_K, \nabla v)_K \\ &\stackrel{(80)}{=} \stackrel{(81)}{=} \max_{\substack{v \in H_*^1(K) \\ \|\nabla v\|_K=1}} (\nabla \psi_{J,\mathbf{a}} \cdot (\mathbf{v}_J - \mathbf{\Pi}_{K,0}(\mathbf{v}_J|_K)), v)_K \\ &\leq \max_{\substack{v \in H_*^1(K) \\ \|\nabla v\|_K=1}} \left\{ \|\nabla \psi_{J,\mathbf{a}}\|_{K,\infty} \|\mathbf{v}_J - \mathbf{\Pi}_{K,0}(\mathbf{v}_J|_K)\|_K \frac{h_K}{\pi} \|\nabla v\|_K \right\} \\ &= \|\nabla \psi_{J,\mathbf{a}}\|_{K,\infty} \|\mathbf{v}_J - \mathbf{\Pi}_{K,0}(\mathbf{v}_J|_K)\|_K \frac{h_K}{\pi} \\ &\lesssim \|\mathbf{v}_J - \mathbf{\Pi}_{K,0}(\mathbf{v}_J|_K)\|_K \leq \|\mathbf{v}_J\|_K, \end{aligned} \quad (82)$$

where the last but one estimate follows as $\|\nabla \psi_{J,\mathbf{a}}\|_{K,\infty} \lesssim h_K^{-1}$, where the hidden constant only depends on the mesh shape regularity, and the last estimate from the stability of the $[L^2(K)]^d$ -orthogonal projection. This finally leads to the desired stability

$$\begin{aligned} \|\boldsymbol{\delta}_{J,\mathbf{a}}\|_K &\leq \|\boldsymbol{\delta}_{J,\mathbf{a}} - (\mathbf{I}_{K,p}^{RT}((\psi_{J,\mathbf{a}} \mathbf{v}_J)|_K) - \boldsymbol{\delta}_{J,0}^{\mathbf{a}})\|_K + \|\mathbf{I}_{K,p}^{RT}((\psi_{J,\mathbf{a}} \mathbf{v}_J)|_K) - \boldsymbol{\delta}_{J,0}^{\mathbf{a}}\|_K \\ &\stackrel{(82)}{\stackrel{(71a)}}{\lesssim} \|\mathbf{v}_J\|_K + \|\mathbf{I}_{K,p}^{RT}((\psi_{J,\mathbf{a}} \mathbf{v}_J)|_K)\|_K + \|\mathbf{I}_{K,0}^{RT}((\psi_{J,\mathbf{a}} \mathbf{v}_J)|_K)\|_K \lesssim 3\|\mathbf{v}_J\|_K, \end{aligned} \quad (83)$$

where we have also used the fact that $\|\psi_{J,\mathbf{a}}\|_{K,\infty} = 1$ and the stability of the elementwise Raviart–Thomas interpolant defined in (69), which brings the dependence of the hidden constant on the polynomial degree p .

Step 5: Decomposition property (68a). It remains to show that the sum of the contributions we introduced indeed gives the original $\mathbf{v}_J \in \mathbf{V}_J^0$, i.e., the equality

$$\sum_{\mathbf{a} \in \mathcal{V}_J} \boldsymbol{\delta}_{J,\mathbf{a}} = \mathbf{v}_J - \boldsymbol{\delta}_{J,0}, \quad (84)$$

where $\boldsymbol{\delta}_{J,0}$ is the global lowest-order contribution (71b) and $\boldsymbol{\delta}_{J,\mathbf{a}}$ for $\mathbf{a} \in \mathcal{V}_J$ are the local high-order contributions (75). First, note that for all mesh elements $K \in \mathcal{T}_J$, there holds

$$\begin{aligned} \left(\sum_{\mathbf{a} \in \mathcal{V}_J} \boldsymbol{\delta}_{J,\mathbf{a}} \right) |_{K \cdot \mathbf{n}} &\stackrel{(75)}{=} \sum_{\mathbf{a} \in \mathcal{V}_J} (\mathbf{I}_{K,p}^{RT}((\psi_{J,\mathbf{a}} \mathbf{v}_J)|_K) - \boldsymbol{\delta}_{J,0}^{\mathbf{a}}) |_{K \cdot \mathbf{n}} \\ &\stackrel{(71a)}{=} (\mathbf{I}_{K,p}^{RT}(\mathbf{v}_J|_K) - \boldsymbol{\delta}_{J,0}) |_{K \cdot \mathbf{n}} = (\mathbf{v}_J - \boldsymbol{\delta}_{J,0}) |_{K \cdot \mathbf{n}}, \end{aligned} \quad (85)$$

also using that $\mathbf{I}_{K,p}^{RT}$ from (69) is linear and projector. Thus, the functions on both sides of (84) have the same normal components on all mesh faces. Next, using that \mathbf{v}_J is divergence-free, we obtain

$$\nabla \cdot \left(\sum_{\mathbf{a} \in \mathcal{V}_J} \delta_{J,\mathbf{a}} \right) = \sum_{\mathbf{a} \in \mathcal{V}_J} \nabla \cdot \delta_{J,\mathbf{a}} \stackrel{(75)}{=} 0 \stackrel{(72)}{=} \nabla \cdot (\mathbf{v}_J - \delta_{J,0}). \quad (86)$$

Thus, the functions on both sides of (84) have the same divergence.

Thanks to (75), for all $K \in \mathcal{T}_J$, there holds

$$(\delta_{J,\mathbf{a}} - (\mathbf{I}_{K,p}^{RT}((\psi_{J,\mathbf{a}}\mathbf{v}_J)|_K) - \delta_{J,0}^{\mathbf{a}}), \mathbf{w}_J)_K = 0 \quad \forall \mathbf{w}_J \in \mathbf{RT}_p(K), \nabla \cdot \mathbf{w}_J = 0, \mathbf{w}_J \cdot \mathbf{n} = 0.$$

Summing over all vertices, together with the patchwise construction (71b) and the fact that the hat functions form a partition of unity, i.e., $\sum_{\mathbf{a} \in \mathcal{V}_J} \psi_{J,\mathbf{a}} = 1$, leads to

$$\begin{aligned} 0 &= \left(\sum_{\mathbf{a} \in \mathcal{V}_J} (\delta_{J,\mathbf{a}} - (\mathbf{I}_{K,p}^{RT}((\psi_{J,\mathbf{a}}\mathbf{v}_J)|_K) - \delta_{J,0}^{\mathbf{a}})), \mathbf{w}_J \right)_K \\ &= \left(\sum_{\mathbf{a} \in \mathcal{V}_J} \delta_{J,\mathbf{a}} - (\mathbf{I}_{K,p}^{RT}(\mathbf{v}_J|_K) - \delta_{J,0}), \mathbf{w}_J \right)_K \\ &= \left(\sum_{\mathbf{a} \in \mathcal{V}_J} \delta_{J,\mathbf{a}} - (\mathbf{v}_J - \delta_{J,0}), \mathbf{w}_J \right)_K \quad \forall \mathbf{w}_J \in \mathbf{RT}_p(K), \nabla \cdot \mathbf{w}_J = 0, \mathbf{w}_J \cdot \mathbf{n} = 0. \end{aligned} \quad (87)$$

Thus, the difference of the functions on both sides of (84) is elementwise orthogonal to normal-component-free and divergence-free functions. Consequently, (85)–(87) together yield the desired decomposition (68a).

Step 6: Stability property (68b). Using the results of steps 2 and 4, one readily obtains

$$\|\delta_{J,0}\|^2 + \sum_{\mathbf{a} \in \mathcal{V}_J} \|\delta_{J,\mathbf{a}}\|_{\omega_{\mathbf{a}}}^2 \stackrel{(74)}{\lesssim} \|\mathbf{v}_J\|^2 + \sum_{\mathbf{a} \in \mathcal{V}_J} \sum_{K \in \mathcal{T}_J} \|\delta_{J,\mathbf{a}}\|_K^2 \stackrel{(83)}{\lesssim} \|\mathbf{v}_J\|^2.$$

Therefrom, the desired stability property (68b) follows taking into account the variations of the diffusion coefficient \mathbf{K} . □

8.4 Multilevel stable decomposition for lowest-order divergence-free Raviart–Thomas piecewise polynomials in three space dimensions

After having obtained a one-level high-order stable decomposition in Lemma 8.3, we decompose further its global lowest-order contribution in a stable multilevel way. Recall the notations \mathbf{V}_j^0 from (20) and $\mathbf{V}_j^{\mathbf{a},0}$ from (23).

Lemma 8.4 (Multilevel lowest-order stable decomposition of \mathbf{V}_j^0 in three space dimensions). *Let either Assumption 3.1 or Assumption 3.2 hold. Assume moreover that $d = 3$. Let the polynomial degree $p = 0$. Then, for any $\mathbf{v}_J \in \mathbf{V}_J^0$, there exist $\mathbf{v}_0 \in \mathbf{V}_0^0$ (global coarse-grid component) and $\mathbf{v}_{j,\mathbf{a}} \in \mathbf{V}_j^{\mathbf{a},0}$, $\mathbf{a} \in \mathcal{V}_j$, (levelwise and local patchwise components) such that*

$$\mathbf{v}_J = \mathbf{v}_0 + \sum_{j=1}^J \sum_{\mathbf{a} \in \mathcal{V}_j} \mathbf{v}_{j,\mathbf{a}} \quad (88a)$$

stable as

$$\|\mathbf{K}^{-1/2}\mathbf{v}_0\|^2 + \sum_{j=1}^J \sum_{\mathbf{a} \in \mathcal{V}_j} \|\mathbf{K}^{-1/2}\mathbf{v}_{j,\mathbf{a}}\|_{\omega_j^{\mathbf{a}}}^2 \leq C_{\text{ML}}^2 \|\mathbf{K}^{-1/2}\mathbf{v}_J\|^2, \quad (88b)$$

where the constant C_{ML} only depends on mesh-geometry parameters $\kappa_{\mathcal{T}}$, C_{qu} and C_{ref} or C_{qu}^0 and $C_{\text{loc,qu}}$, and the diffusion inhomogeneity or anisotropy ratio $\Lambda_{\text{max}}/\Lambda_{\text{min}}$. In particular, C_{ML} is independent of the number of mesh levels J .

Proof. First, using that Ω is homotopic to a ball, we introduce the stable discrete potential $\boldsymbol{\xi}_J \in \mathbf{N}_{J,0}$ (recall (59)) of \mathbf{v}_J using Lemma 8.2. Then, we decompose $\boldsymbol{\xi}_J$ following Hiptmair, Wu, and Zheng [25, Theorem 5.2], which will lead to a stable decomposition of the original \mathbf{v}_J .

We first introduce some notation. Let \mathcal{E}_j^+ denote the set of new edges arising in the j -th mesh refinement step and their immediate neighboring edges. Let $\phi_{j,e}$ be the lowest-order basis function of the Nédélec space $\mathbf{N}_{j,0}$ associated to the edge $e \in \mathcal{E}_j^+$ and let $\omega_j^e := \text{supp}(\phi_{j,e})$. Similarly, let \mathcal{V}_j^+ denote the set of new vertices arising in the j -th mesh refinement step and their immediate neighboring vertices. Denote by $\psi_{j,\mathbf{a}}$ the piecewise linear hat function which takes value one at the vertex $\mathbf{a} \in \mathcal{V}_j$ and vanishes in all other vertices of level j . Then, from [25, Theorem 5.2], for any $\boldsymbol{\xi}_J \in \mathbf{N}_{J,0}$, there exist $\boldsymbol{\xi}_0 \in \mathbf{N}_{0,0}$, $\boldsymbol{\xi}_{j,e} \in \text{span}\{\phi_{j,e}\}$ with $e \in \mathcal{E}_j^+$, $\xi_{j,\mathbf{a}} \in \text{span}\{\psi_{j,\mathbf{a}}\}$ with $\mathbf{a} \in \mathcal{V}_j^+$, $1 \leq j \leq J$, such that the decomposition

$$\boldsymbol{\xi}_J = \boldsymbol{\xi}_0 + \sum_{j=1}^J \sum_{e \in \mathcal{E}_j^+} \boldsymbol{\xi}_{j,e} + \sum_{j=1}^J \sum_{\mathbf{a} \in \mathcal{V}_j^+} \nabla \xi_{j,\mathbf{a}} \quad (89a)$$

is stable as

$$\|\boldsymbol{\xi}_0\|_{\mathbf{H}(\text{curl};\Omega)}^2 + \sum_{j=1}^J \sum_{e \in \mathcal{E}_j^+} \|\boldsymbol{\xi}_{j,e}\|_{\mathbf{H}(\text{curl};\omega_j^e)}^2 + \sum_{j=1}^J \sum_{\mathbf{a} \in \mathcal{V}_j^+} \|\nabla \xi_{j,\mathbf{a}}\|_{\omega_j^{\mathbf{a}}}^2 \leq C_{3\text{D}}^2 \|\boldsymbol{\xi}_J\|_{\mathbf{H}(\text{curl};\Omega)}^2, \quad (89b)$$

where $\|\boldsymbol{\zeta}\|_{\mathbf{H}(\text{curl};\omega)}^2 := \|\boldsymbol{\zeta}\|_{\omega}^2 + \|\nabla \times \boldsymbol{\zeta}\|_{\omega}^2$ for any $\boldsymbol{\zeta} \in \mathbf{H}(\text{curl};\omega)$, $\omega \subset \mathbb{R}^d$.

Let the edges in \mathcal{E}_j^+ be re-indexed by associating them to patches such that any edge is only counted once and such that each edge basis function has tangential trace zero on the boundary of the patch it is associated to. We write $\mathcal{E}_j^+ = \cup_{\mathbf{a} \in \mathcal{V}_j} \mathcal{E}_j^{\mathbf{a}}$, which gives $\sum_{\mathbf{a} \in \mathcal{V}_j} \sum_{e \in \mathcal{E}_j^{\mathbf{a}}} = \sum_{e \in \mathcal{E}_j^+}$. Then, we apply the decomposition (89a) to (60), leading to

$$\mathbf{v}_J = \nabla \times \boldsymbol{\xi}_J = \nabla \times \boldsymbol{\xi}_0 + \sum_{j=1}^J \sum_{e \in \mathcal{E}_j^+} \nabla \times \boldsymbol{\xi}_{j,e} + 0 = \mathbf{v}_0 + \sum_{j=1}^J \sum_{\mathbf{a} \in \mathcal{V}_j} \mathbf{v}_{j,\mathbf{a}},$$

with $\mathbf{v}_0 := \nabla \times \boldsymbol{\xi}_0 \in \mathbf{V}_0^0$ and $\mathbf{v}_{j,\mathbf{a}} := \sum_{e \in \mathcal{E}_j^{\mathbf{a}}} \nabla \times \boldsymbol{\xi}_{j,e} \in \mathbf{V}_j^{\mathbf{a},0}$. Finally, this decomposition is stable as

$$\begin{aligned} \|\mathbf{v}_0\|^2 + \sum_{j=1}^J \sum_{\mathbf{a} \in \mathcal{V}_j} \|\mathbf{v}_{j,\mathbf{a}}\|_{\omega_j^{\mathbf{a}}}^2 &= \|\nabla \times \boldsymbol{\xi}_0\|^2 + \sum_{j=1}^J \sum_{\mathbf{a} \in \mathcal{V}_j} \left\| \sum_{e \in \mathcal{E}_j^{\mathbf{a}}} \nabla \times \boldsymbol{\xi}_{j,e} \right\|_{\omega_j^{\mathbf{a}}}^2 \\ &\lesssim \|\nabla \times \boldsymbol{\xi}_0\|^2 + \sum_{j=1}^J \sum_{e \in \mathcal{E}_j^+} \|\nabla \times \boldsymbol{\xi}_{j,e}\|_{\omega_j^e}^2 \\ &\stackrel{(89b)}{\leq} C_{3\text{D}}^2 (\|\boldsymbol{\xi}_J\|^2 + \|\nabla \times \boldsymbol{\xi}_J\|^2) \stackrel{(60)}{\leq} C_{3\text{D}}^2 (C_{\text{pot}}^2 + 1) \|\mathbf{v}_J\|^2. \end{aligned}$$

The desired result (88b) is then obtained after taking into consideration the variations of the diffusion coefficient \mathbf{K} . \square

8.5 Multilevel stable decomposition for high-order divergence-free Raviart–Thomas piecewise polynomials

We can now finally present our stable multilevel decomposition of the space \mathbf{V}_J^0 from (20):

Proposition 8.5 (Multilevel high-order stable decomposition of \mathbf{V}_J^0). *Let either Assumption 3.1 or Assumption 3.2 hold. Then for any $\mathbf{v}_J \in \mathbf{V}_J^0$, there exist $\mathbf{v}_0 \in \mathbf{V}_0^0 \cap \mathbf{RT}_0(\mathcal{T}_0)$ (global coarse-grid lowest-order component) and $\mathbf{v}_{j,\mathbf{a}} \in \mathbf{V}_j^{\mathbf{a},0}$, $1 \leq j \leq J$, $\mathbf{a} \in \mathcal{V}_j$, (levelwise and local patchwise high-order components) such that the decomposition*

$$\mathbf{v}_J = \mathbf{v}_0 + \sum_{j=1}^J \sum_{\mathbf{a} \in \mathcal{V}_j} \mathbf{v}_{j,\mathbf{a}} \quad (90a)$$

is stable as

$$\|\mathbf{K}^{-1/2} \mathbf{v}_0\|^2 + \sum_{j=1}^J \sum_{\mathbf{a} \in \mathcal{V}_j} \|\mathbf{K}^{-1/2} \mathbf{v}_{j,\mathbf{a}}\|_{\omega_j^{\mathbf{a}}}^2 \leq C_{\text{SD}}^2 \|\mathbf{K}^{-1/2} \mathbf{v}_J\|^2, \quad (90b)$$

where the positive constant C_{SD} only depends on the mesh-geometry parameters $\kappa_{\mathcal{T}}$, C_{qu} and C_{ref} or C_{qu}^0 and $C_{\text{loc,qu}}$, the diffusion inhomogeneity or anisotropy ratio $\Lambda_{\text{max}}/\Lambda_{\text{min}}$, and, if $d = 3$, possibly on the polynomial degree p . In particular, C_{SD} is independent of the number of mesh levels J .

Proof of Proposition 8.5 for $d = 2$. The construction of the stable decomposition for $d = 2$ uses the property that, since Ω is homotopic to a ball, there exists a discrete stream-function space

$$S_J := \mathbb{P}_{p+1}(\mathcal{T}_J) \cap H_0^1(\Omega) \quad (91)$$

such that

$$\mathbf{V}_J^0 = \nabla \times S_J, \quad (92)$$

see e.g., Boffi, Brezzi, and Fortin. [3, Corollary 2.3.2]. Here, we use the notation

$$\nabla \times s = \begin{pmatrix} s_y \\ -s_x \end{pmatrix} = \begin{pmatrix} 0 & 1 \\ -1 & 0 \end{pmatrix} \begin{pmatrix} s_x \\ s_y \end{pmatrix} = \begin{pmatrix} 0 & 1 \\ -1 & 0 \end{pmatrix} \nabla s. \quad (93)$$

Since for all $\mathbf{v}_J, \mathbf{w}_J \in \mathbf{V}_J^0$, by (92), there is $s_J, \theta_J \in S_J$ such that $\mathbf{v}_J = \nabla \times s_J$ and $\mathbf{w}_J = \nabla \times \theta_J$, we obtain from (93) that

$$(\mathbf{K}^{-1} \mathbf{v}_J, \mathbf{w}_J) = (\mathbf{K}^{-1} \nabla \times s_J, \nabla \times \theta_J) = (\mathcal{A} \nabla s_J, \nabla \theta_J) \quad (94)$$

for $\mathcal{A} := \begin{pmatrix} 0 & -1 \\ 1 & 0 \end{pmatrix} \mathbf{K}^{-1} \begin{pmatrix} 0 & 1 \\ -1 & 0 \end{pmatrix}$. In particular, note that $(\mathbf{K}^{-1} \mathbf{v}_J, \mathbf{w}_J) = (\nabla s_J, \nabla \theta_J)$ when $\mathbf{K} = I$. Similar properties obviously hold on patches as well.

Let us now show (90) for $d = 2$. Let $\mathbf{v}_J \in \mathbf{V}_J^0$. By (92), there is $v_J \in S_J$ such that

$$\mathbf{v}_J = \nabla \times v_J. \quad (95)$$

We can now use the stable decomposition of Lemma 8.1 for v_J : there exist $v_0 \in S_0^1$ and $v_{j,\mathbf{a}} \in S_j^{\mathbf{a}}$, $1 \leq j \leq J$, $\mathbf{a} \in \mathcal{V}_j$, such that $v_J = v_0 + \sum_{j=1}^J \sum_{\mathbf{a} \in \mathcal{V}_j} v_{j,\mathbf{a}}$ and (57) holds. Define

$$\mathbf{v}_0 := \nabla \times v_0 \quad \text{and} \quad \mathbf{v}_{j,\mathbf{a}} := \nabla \times v_{j,\mathbf{a}}. \quad (96)$$

Since $\mathbf{V}_0^0 = \nabla \times S_0^1$ and $\mathbf{V}_j^{\mathbf{a},0} = \nabla \times S_j^{\mathbf{a}}$, $1 \leq j \leq J$, $\mathbf{a} \in \mathcal{V}_j$, we have $\mathbf{v}_0 \in \mathbf{V}_0^0$ and $\mathbf{v}_{j,\mathbf{a}} \in \mathbf{V}_j^{\mathbf{a},0}$. Note that by applying $\nabla \times$ on both sides of (57a), we have

$$\mathbf{v}_J = \mathbf{v}_0 + \sum_{j=1}^J \sum_{\mathbf{a} \in \mathcal{V}_j} \mathbf{v}_{j,\mathbf{a}}, \quad \mathbf{v}_0 \in \mathbf{V}_0^0, \quad \mathbf{v}_{j,\mathbf{a}} \in \mathbf{V}_j^{\mathbf{a},0},$$

which is the first part (90a) of the result we want to prove. Next, note that

$$\begin{aligned} \|\mathbf{v}_0\|^2 + \sum_{j=1}^J \sum_{\mathbf{a} \in \mathcal{V}_j} \|\mathbf{v}_{j,\mathbf{a}}\|_{\omega_j^{\mathbf{a}}}^2 &\stackrel{(96)}{=} \|\nabla \times v_0\|^2 + \sum_{j=1}^J \sum_{\mathbf{a} \in \mathcal{V}_j} \|\nabla \times v_{j,\mathbf{a}}\|_{\omega_j^{\mathbf{a}}}^2 \\ &\stackrel{(94)}{=} \|\nabla v_0\|^2 + \sum_{j=1}^J \sum_{\mathbf{a} \in \mathcal{V}_j} \|\nabla v_{j,\mathbf{a}}\|_{\omega_j^{\mathbf{a}}}^2 \\ &\stackrel{(57b)}{\leq} C_{\text{SD}}^2 \|\nabla v_J\|^2 \stackrel{(94)}{=} C_{\text{SD}}^2 \|\nabla \times v_J\|^2 \stackrel{(95)}{=} C_{\text{SD}}^2 \|\mathbf{v}_J\|^2. \end{aligned}$$

Finally, the result (90b) follows once we take into account the variations of the diffusion coefficient \mathbf{K} . □

Proof of Proposition 8.5 for $d = 3$. Let $\mathbf{v}_J \in \mathbf{V}_J^0$. We first apply the one-level high-order decomposition of Lemma 8.3. This gives us $\boldsymbol{\alpha}_J \in \mathbf{V}_J^0 \cap \mathbf{RT}_0(\mathcal{T}_J)$ and $\boldsymbol{\delta}_{J,\mathbf{a}} \in \mathbf{V}_J^{\mathbf{a},0}$, $\mathbf{a} \in \mathcal{V}_J$, such that

$$\mathbf{v}_J = \boldsymbol{\alpha}_J + \sum_{\mathbf{a} \in \mathcal{V}_J} \boldsymbol{\delta}_{J,\mathbf{a}}$$

with the stability bound (68b). Now, we decompose $\boldsymbol{\alpha}_J$ thanks to Lemma 8.4. This gives $\boldsymbol{\alpha}_0 \in \mathbf{V}_0^0 \cap \mathbf{RT}_0(\mathcal{T}_0)$ and $\boldsymbol{\delta}_{J,0}^{\mathbf{a}} \in \mathbf{V}_J^{\mathbf{a},0} \cap \mathbf{RT}_0(\mathcal{T}_a)$, $\mathbf{a} \in \mathcal{V}_j$, such that

$$\boldsymbol{\alpha}_J = \boldsymbol{\alpha}_0 + \sum_{j=1}^J \sum_{\mathbf{a} \in \mathcal{V}_j} \boldsymbol{\delta}_{J,0}^{\mathbf{a}}$$

and the stability bound (88b). Define $\mathbf{v}_0 := \boldsymbol{\alpha}_0 \in \mathbf{V}_0^0 \cap \mathbf{RT}_0(\mathcal{T}_0)$, $\mathbf{v}_{j,\mathbf{a}} := \boldsymbol{\delta}_{J,0}^{\mathbf{a}} \in \mathbf{V}_j^{\mathbf{a},0} \cap \mathbf{RT}_0(\mathcal{T}_a)$ for $1 \leq j \leq J-1$, and $\mathbf{v}_{J,\mathbf{a}} := \boldsymbol{\delta}_{J,0}^{\mathbf{a}} + \boldsymbol{\delta}_{J,\mathbf{a}} \in \mathbf{V}_J^{\mathbf{a},0}$. This yields the decomposition (90a). The stability (90b) follows by

$$\begin{aligned} \|\mathbf{K}^{-1/2} \mathbf{v}_0\|^2 + \sum_{j=1}^J \sum_{\mathbf{a} \in \mathcal{V}_j} \|\mathbf{K}^{-1/2} \mathbf{v}_{j,\mathbf{a}}\|_{\omega_j^{\mathbf{a}}}^2 \\ = \|\mathbf{K}^{-1/2} \boldsymbol{\alpha}_0\|^2 + \sum_{j=1}^{J-1} \sum_{\mathbf{a} \in \mathcal{V}_j} \|\mathbf{K}^{-1/2} \boldsymbol{\delta}_{J,0}^{\mathbf{a}}\|_{\omega_j^{\mathbf{a}}}^2 + \sum_{\mathbf{a} \in \mathcal{V}_J} \|\mathbf{K}^{-1/2} (\boldsymbol{\delta}_{J,0}^{\mathbf{a}} + \boldsymbol{\delta}_{J,\mathbf{a}})\|_{\omega_j^{\mathbf{a}}}^2 \\ \stackrel{(88b)}{\leq} 2C_{\text{ML}}^2 \|\mathbf{K}^{-1/2} \boldsymbol{\alpha}_J\|^2 + 2 \sum_{\mathbf{a} \in \mathcal{V}_J} \|\mathbf{K}^{-1/2} \boldsymbol{\delta}_{J,\mathbf{a}}\|_{\omega_j^{\mathbf{a}}}^2 \stackrel{(68b)}{\leq} 2C_{\text{OL}}^2 C_{\text{ML}}^2 \|\mathbf{K}^{-1/2} \mathbf{v}_J\|^2. \end{aligned}$$

□

Remark 8.6. Note that in [19, 20] a stable decomposition of the form (90) was presented in two space dimensions and for the case of quadrilateral and triangular elements, respectively. In [9], the stable decomposition was extended to three space dimensions for the case of tetrahedral elements and lowest-order polynomial degree. Thus, the result of Proposition 8.5 is more general as it holds for $d \in \{2, 3\}$ and polynomial degree $p \geq 0$.

9 Proof of Theorem 6.2

In this section, we present a proof of Theorem 6.2. We rely for this purpose on the stable decomposition result of Proposition 8.5 established above. First, we present a remark:

Remark 9.1 (Lower bound on the optimal step-sizes). *In the multilevel setting, as in [34, Lemma 10.1], (27) together with a patch overlap argument yields*

$$\|\mathbf{K}^{-1/2} \boldsymbol{\rho}_j^i\|^2 \leq (d+1) \sum_{\mathbf{a} \in \mathcal{V}_j} \|\mathbf{K}^{-1/2} \boldsymbol{\rho}_{j,\mathbf{a}}^i\|_{\omega_j^{\mathbf{a}}}^2. \quad (97)$$

A direct consequence of (97) and (34), together with the definition $\lambda_j^i = 1$ when $j = 0$ or $\boldsymbol{\rho}_j^i = 0$, is

$$\lambda_j^i \geq \frac{1}{d+1} \quad 0 \leq j \leq J. \quad (98)$$

Similarly, in the domain decomposition setting, (41) together with a patch overlap on the coarse mesh \mathcal{T}_H yields

$$\|\mathbf{K}^{-1/2} \boldsymbol{\rho}_h^i\|^2 \leq (d+1) \sum_{\mathbf{a} \in \mathcal{V}_H} \|\mathbf{K}^{-1/2} \boldsymbol{\rho}_{h,\mathbf{a}}^i\|_{\omega_H^{\mathbf{a}}}^2. \quad (99)$$

Thus, from (99) and (45), together with the definition $\lambda_h^i = 1$ when $\boldsymbol{\rho}_h^i = 0$,

$$\lambda_h^i \geq \frac{1}{d+1}. \quad (100)$$

9.1 Multilevel setting

We can now present the proof of Theorem 6.2 for the estimator built in Algorithm 4.2.

Proof of Theorem 6.2 (multilevel setting). The proof follows closely the proof of [34, Theorem 6.6], thus only the main steps are presented here. Using the stable decomposition (90a) applied to the error gives

$$\mathbf{u}_J - \mathbf{u}_J^i = \mathbf{v}_0 + \sum_{j=1}^J \sum_{\mathbf{a} \in \mathcal{V}_j} \mathbf{v}_{j,\mathbf{a}}. \quad (101)$$

Since $\mathbf{u}_J - \mathbf{u}_J^i \in \mathbf{V}_J^0$ and using (13) as well as the construction of the multilevel solver, one obtains

$$\begin{aligned}
\|\mathbf{K}^{-1/2}(\mathbf{u}_J - \mathbf{u}_J^i)\|^2 &\stackrel{(13)}{=} -(\mathbf{K}^{-1}\mathbf{u}_J^i, \mathbf{u}_J - \mathbf{u}_J^i) \stackrel{(101)}{=} -\left(\mathbf{K}^{-1}\mathbf{u}_J^i, \mathbf{v}_0 + \sum_{j=1}^J \sum_{\mathbf{a} \in \mathcal{V}_j} \mathbf{v}_{j,\mathbf{a}}\right) \\
&\stackrel{(24)}{=} (\mathbf{K}^{-1}\boldsymbol{\rho}_0^i, \mathbf{v}_0) - \sum_{j=1}^J \sum_{\mathbf{a} \in \mathcal{V}_j} (\mathbf{K}^{-1}\mathbf{u}_J^i, \mathbf{v}_{j,\mathbf{a}})_{\omega_j^{\mathbf{a}}} \\
&\stackrel{(32)}{=} (\mathbf{K}^{-1}\boldsymbol{\rho}_0^i, \mathbf{v}_0) + \sum_{j=1}^J \sum_{\mathbf{a} \in \mathcal{V}_j} (\mathbf{K}^{-1}\boldsymbol{\rho}_{j,\mathbf{a}}^i, \mathbf{v}_{j,\mathbf{a}})_{\omega_j^{\mathbf{a}}} \\
&\quad + \sum_{j=1}^J \sum_{m=0}^{j-1} \sum_{\mathbf{a} \in \mathcal{V}_j} \lambda_m^i (\mathbf{K}^{-1}\boldsymbol{\rho}_m^i, \mathbf{v}_{j,\mathbf{a}})_{\omega_j^{\mathbf{a}}}
\end{aligned}$$

In the same spirit of [34, Proof of Theorem 6.6, page S138], one can use (98) together with Young's inequalities and the stability of the decomposition (90b) to show that there holds

$$\begin{aligned}
\|\mathbf{K}^{-1/2}(\mathbf{u}_J - \mathbf{u}_J^i)\|^2 &\leq C^2 \left(\|\mathbf{K}^{-1/2}\boldsymbol{\rho}_0^i\|^2 + \sum_{j=1}^J \lambda_j^i \sum_{\mathbf{a} \in \mathcal{V}_j} \|\mathbf{K}^{-1/2}\boldsymbol{\rho}_{j,\mathbf{a}}^i\|_{\omega_j^{\mathbf{a}}}^2 \right) \\
&\stackrel{(47)}{=} C^2 (\eta_{\text{alg}}^i)^2,
\end{aligned} \tag{102}$$

where C only depends on C_{SD} of (90b) and at most linearly on the number of mesh levels J . \square

9.2 Two-level domain decomposition setting

We now proceed to the proof of Theorem 6.2 for the estimator built in Algorithm 5.1. First, we present a few preparatory steps that will allow us to re-use the results we presented in the multilevel setting.

Our goal is to write a multilevel presentation of the algebraic residual lifting $\boldsymbol{\rho}_{h,\mathbf{a}}^i \in \mathbf{V}_h^{\mathbf{a},0}$ computed by solving the subdomain problem (40) on $\omega_H^{\mathbf{a}}$. Recall that $\omega_H^{\mathbf{a}}$ is the open subdomain corresponding to the coarse-grid patch $\mathcal{T}_0^{\mathbf{a}}$. For the purpose of the analysis only, define the local MFE space on $\omega_H^{\mathbf{a}}$ associated with the intermediate mesh levels \mathcal{T}_j , $1 \leq j \leq J$, as

$$\mathbf{V}_{j,H}^{\mathbf{a}} := \{\mathbf{v}_j \in \mathbf{V}_j|_{\omega_H^{\mathbf{a}}}, \mathbf{v}_j \cdot \mathbf{n} = 0 \text{ on } \partial\omega_H^{\mathbf{a}}\}. \tag{103}$$

In contrast to the spaces $\mathbf{V}_j^{\mathbf{a}}$ from Section 4.1, which are defined on the j -level (small) patches $\omega_j^{\mathbf{a}}$, we stress that the spaces $\mathbf{V}_{j,H}^{\mathbf{a}}$ are defined on the subdomains (large patches) $\omega_H^{\mathbf{a}}$ and their fine meshes \mathcal{T}_j ; there are much fewer spaces $\mathbf{V}_{j,H}^{\mathbf{a}}$ than there are spaces $\mathbf{V}_j^{\mathbf{a}}$ but the spaces $\mathbf{V}_{j,H}^{\mathbf{a}}$ have much higher dimension than $\mathbf{V}_j^{\mathbf{a}}$. Finally, define the divergence-free subspace of $\mathbf{V}_{j,H}^{\mathbf{a}}$,

$$\mathbf{V}_{j,H}^{\mathbf{a},0} = \{\mathbf{v}_{j,\mathbf{a}} \in \mathbf{V}_{j,H}^{\mathbf{a}}, \nabla \cdot \mathbf{v}_{j,\mathbf{a}} = 0\}. \tag{104}$$

Let a coarse mesh vertex $\mathbf{a} \in \mathcal{V}_H$ be fixed. We now consider an orthogonal multilevel decomposition of $\boldsymbol{\rho}_{h,\mathbf{a}}^i \in \mathbf{V}_h^{\mathbf{a},0}$ from (40) on the subdomain $\omega_H^{\mathbf{a}}$. For $1 \leq j \leq J$, define for (analysis purposes, not constructed in practice) $\boldsymbol{\rho}_{j,\mathbf{a}}^i \in \mathbf{V}_{j,H}^{\mathbf{a},0}$ as the solutions to

$$(\mathbf{K}^{-1}\boldsymbol{\rho}_{j,\mathbf{a}}^i, \mathbf{v}_{j,\mathbf{a}})_{\omega_H^{\mathbf{a}}} = -(\mathbf{K}^{-1}\mathbf{u}_H^i, \mathbf{v}_{j,\mathbf{a}})_{\omega_H^{\mathbf{a}}} - \sum_{m=1}^{j-1} (\mathbf{K}^{-1}\boldsymbol{\rho}_{m,\mathbf{a}}^i, \mathbf{v}_{j,\mathbf{a}})_{\omega_H^{\mathbf{a}}} \quad \forall \mathbf{v}_{j,\mathbf{a}} \in \mathbf{V}_{j,H}^{\mathbf{a},0}, \quad \forall 1 \leq j \leq J. \tag{105}$$

Taking above $j = J$ and noting that $\mathbf{V}_{J,H}^{\mathbf{a},0} = \mathbf{V}_h^{\mathbf{a},0}$ in our notation, it follows that

$$\sum_{j=1}^J (\mathbf{K}^{-1} \boldsymbol{\rho}_{j,\mathbf{a}}^i, \mathbf{v}_{h,\mathbf{a}})_{\omega_H^{\mathbf{a}}} = -(\mathbf{K}^{-1} \mathbf{u}_H^i, \mathbf{v}_{h,\mathbf{a}})_{\omega_H^{\mathbf{a}}} \quad \forall \mathbf{v}_{h,\mathbf{a}} \in \mathbf{V}_h^{\mathbf{a},0},$$

which, together with (40), implies that

$$\boldsymbol{\rho}_{h,\mathbf{a}}^i = \sum_{j=1}^J \boldsymbol{\rho}_{j,\mathbf{a}}^i, \quad (106)$$

so that $\boldsymbol{\rho}_{j,\mathbf{a}}^i$ decompose $\boldsymbol{\rho}_{h,\mathbf{a}}^i$. Moreover, this decomposition is indeed orthogonal:

$$(\mathbf{K}^{-1} \boldsymbol{\rho}_{j,\mathbf{a}}^i, \boldsymbol{\rho}_{m,\mathbf{a}}^i)_{\omega_H^{\mathbf{a}}} = 0, \quad 1 \leq j, m \leq J, j \neq m, \quad (107)$$

and

$$\|\mathbf{K}^{-1/2} \boldsymbol{\rho}_{h,\mathbf{a}}^i\|_{\omega_H^{\mathbf{a}}}^2 = \sum_{j=1}^J \|\mathbf{K}^{-1/2} \boldsymbol{\rho}_{j,\mathbf{a}}^i\|_{\omega_H^{\mathbf{a}}}^2. \quad (108)$$

With the above developments, the convergence analysis in the domain decomposition setting is a modification of the multigrid analysis presented in the previous Section 9.1. The key point is that the multilevel representation (106) allows us to use the stable decomposition from Proposition 8.5:

Proof of Theorem 6.2 (two-level domain decomposition setting). The proof here is more similar to [33, Lemma 7.7], since the patches we are considering are bigger than the ones used in the stable decomposition of Proposition 8.5. Thus, we first define, for every $j \in \{1, \dots, J\}$ and $\mathbf{a} \in \mathcal{V}_H$, the set $\mathcal{I}_{\mathbf{a},j} \subset \mathcal{V}_j$ containing vertices in \mathcal{T}_j of the interior of the patch $\omega_H^{\mathbf{a}}$ such that $\{\mathcal{I}_{\mathbf{a},j}\}_{\mathbf{a} \in \mathcal{V}_H}$ cover \mathcal{V}_j and are mutually disjoint. Let $\mathbf{v}_{j,\mathbf{a}} \in \mathbf{V}_j^{\mathbf{a},0}$. This allows us to write

$$\sum_{\mathbf{a} \in \mathcal{V}_j} \mathbf{v}_{j,\mathbf{a}} = \sum_{\mathbf{a} \in \mathcal{V}_H} \sum_{\mathbf{b} \in \mathcal{I}_{\mathbf{a},j}} \mathbf{v}_{j,\mathbf{b}}. \quad (109)$$

Moreover, since the vertices of $\mathcal{I}_{\mathbf{a},j}$ are localized in the interior of the patch $\omega_H^{\mathbf{a}}$, we have

$$\sum_{\mathbf{b} \in \mathcal{I}_{\mathbf{a},j}} \mathbf{v}_{j,\mathbf{b}} \in \mathbf{V}_{j,H}^{\mathbf{a},0}. \quad (110)$$

Once again, we use the stable decomposition (90a) applied to the error

$$\mathbf{u}_J - \mathbf{u}_h^i = \mathbf{v}_0 + \sum_{j=1}^J \sum_{\mathbf{a} \in \mathcal{V}_j} \mathbf{v}_{j,\mathbf{a}} \quad (111)$$

and the construction of the multilevel solver

$$\begin{aligned}
& \|\mathbf{K}^{-1/2}(\mathbf{u}_J - \mathbf{u}_h^i)\|^2 \stackrel{(13)}{=} -(\mathbf{K}^{-1}\mathbf{u}_h^i, \mathbf{u}_J - \mathbf{u}_h^i) \stackrel{(111)}{=} -\left(\mathbf{K}^{-1}\mathbf{u}_h^i, \mathbf{v}_0 + \sum_{j=1}^J \sum_{\mathbf{a} \in \mathcal{V}_j} \mathbf{v}_{j,\mathbf{a}}\right) \\
& \stackrel{(38)}{=} (\mathbf{K}^{-1}\boldsymbol{\rho}_H^i, \mathbf{v}_0) - \sum_{j=1}^J \sum_{\mathbf{a} \in \mathcal{V}_j} (\mathbf{K}^{-1}\mathbf{u}_h^i, \mathbf{v}_{j,\mathbf{a}})_{\omega_j^\mathbf{a}} \\
& \stackrel{(39)}{=} (\mathbf{K}^{-1}\boldsymbol{\rho}_H^i, \mathbf{v}_0) - \sum_{j=1}^J \sum_{\mathbf{a} \in \mathcal{V}_j} (\mathbf{K}^{-1}(\mathbf{u}_H^i - \boldsymbol{\rho}_H^i), \mathbf{v}_{j,\mathbf{a}})_{\omega_j^\mathbf{a}} \\
& \stackrel{(109)}{=} (\mathbf{K}^{-1}\boldsymbol{\rho}_H^i, \mathbf{v}_0) - \sum_{j=1}^J \sum_{\mathbf{a} \in \mathcal{V}_H} \left(\mathbf{K}^{-1}(\mathbf{u}_H^i - \boldsymbol{\rho}_H^i), \sum_{\mathbf{b} \in \mathcal{I}_{\mathbf{a},j}} \mathbf{v}_{j,\mathbf{b}}\right)_{\omega_H^\mathbf{a}} \\
& \stackrel{(110)}{=} \stackrel{(105)}{=} (\mathbf{K}^{-1}\boldsymbol{\rho}_H^i, \mathbf{v}_0) + \sum_{j=1}^J \sum_{\mathbf{a} \in \mathcal{V}_H} \left\{ (\mathbf{K}^{-1}\boldsymbol{\rho}_{j,\mathbf{a}}^i, \sum_{\mathbf{b} \in \mathcal{I}_{\mathbf{a},j}} \mathbf{v}_{j,\mathbf{b}})_{\omega_H^\mathbf{a}} \right. \\
& \quad \left. + \sum_{m=1}^{j-1} \left(\mathbf{K}^{-1}\boldsymbol{\rho}_{m,\mathbf{a}}^i, \sum_{\mathbf{b} \in \mathcal{I}_{\mathbf{a},j}} \mathbf{v}_{j,\mathbf{b}}\right)_{\omega_H^\mathbf{a}} + \left(\mathbf{K}^{-1}\boldsymbol{\rho}_H^i, \sum_{\mathbf{b} \in \mathcal{I}_{\mathbf{a},j}} \mathbf{v}_{j,\mathbf{b}}\right)_{\omega_H^\mathbf{a}} \right\}.
\end{aligned}$$

Using Young's inequality and the stability of the decomposition (90b), one can follow the approach of [33, Lemma 7.7] or similarly [34, Proof of Theorem 6.6], to show that there holds

$$\|\mathbf{K}^{-1/2}(\mathbf{u}_J - \mathbf{u}_h^i)\|^2 \leq \tilde{C}^2 \left(\|\mathbf{K}^{-1/2}\boldsymbol{\rho}_H^i\|^2 + \sum_{j=1}^J \sum_{\mathbf{a} \in \mathcal{V}_H} \|\mathbf{K}^{-1/2}\boldsymbol{\rho}_{j,\mathbf{a}}^i\|_{\omega_H^\mathbf{a}}^2 \right), \quad (112)$$

where \tilde{C}^2 only depends on C_{SD} of (90b) and at most linearly on the number of mesh levels J . Finally, we obtain the result

$$\begin{aligned}
\|\mathbf{K}^{-1/2}(\mathbf{u}_J - \mathbf{u}_h^i)\|^2 & \stackrel{(112)}{\leq} \tilde{C}^2 \left(\|\mathbf{K}^{-1/2}\boldsymbol{\rho}_H^i\|^2 + \sum_{j=1}^J \sum_{\mathbf{a} \in \mathcal{V}_H} \|\mathbf{K}^{-1/2}\boldsymbol{\rho}_{j,\mathbf{a}}^i\|_{\omega_H^\mathbf{a}}^2 \right) \\
& \stackrel{(108)}{=} \tilde{C}^2 \left(\|\mathbf{K}^{-1/2}\boldsymbol{\rho}_H^i\|^2 + \sum_{\mathbf{a} \in \mathcal{V}_H} \|\mathbf{K}^{-1/2}\boldsymbol{\rho}_{h,\mathbf{a}}^i\|_{\omega_H^\mathbf{a}}^2 \right) \\
& \stackrel{(100)}{\leq} \tilde{C}^2(d+1) \left(\|\mathbf{K}^{-1/2}\boldsymbol{\rho}_H^i\|^2 + \lambda_h^i \sum_{\mathbf{a} \in \mathcal{V}_H} \|\mathbf{K}^{-1/2}\boldsymbol{\rho}_{h,\mathbf{a}}^i\|_{\omega_H^\mathbf{a}}^2 \right) \\
& \stackrel{(48)}{=} \tilde{C}^2(d+1)(\eta_{\text{alg}}^i)^2.
\end{aligned}$$

□

10 Conclusions

In this work, we have presented an a-posteriori-steered multigrid solver and an a-posteriori-steered two-level domain decomposition method to solve iteratively an algebraic system originating from a saddle-point mixed finite element discretization of a second-order elliptic problem. The update in the solvers is constructed in such way that the norm of its components provides an a posteriori

estimate of the algebraic error. We proved that, in two space dimensions, the a posteriori estimators are efficient independently of the polynomial degree p used in the discretization. In three space dimensions, we could not theoretically establish the p -robustness. This efficiency of the a posteriori estimators leads to the equivalent result of the associated solvers contracting the algebraic error at each iteration, in particular independently of p for the two dimensional case. Though not the topic here, one may also treat the dependency with respect the number of mesh levels J by the so-called local smoothing, see, e.g., Innerberger et al. [27] and the references therein. The idea consists in only solving the local problems associated to degrees of freedom that are new with respect to the previous mesh, which is pertinent in hierarchies leading to graded meshes.

References

- [1] D. N. ARNOLD, R. S. FALK, AND R. WINTHER, *Multigrid in $H(\text{div})$ and $H(\text{curl})$* , Numer. Math., 85 (2000), pp. 197–217.
- [2] M. BENZI, G. H. GOLUB, AND J. LIESEN, *Numerical solution of saddle point problems*, Acta Numer., 14 (2005), pp. 1–137.
- [3] D. BOFFI, F. BREZZI, AND M. FORTIN, *Mixed finite element methods and applications*, vol. 44 of Springer Series in Computational Mathematics, Springer, Heidelberg, 2013.
- [4] S. C. BRENNER, *A multigrid algorithm for the lowest-order Raviart-Thomas mixed triangular finite element method*, SIAM J. Numer. Anal., 29 (1992), pp. 647–678.
- [5] ———, *Fast solvers for mixed finite element methods*, in Mixed finite element technologies, vol. 509 of CISM Courses and Lect., SpringerWienNewYork, Vienna, 2009, pp. 57–88.
- [6] S. C. BRENNER, D.-S. OH, AND L.-Y. SUNG, *Multigrid methods for saddle point problems: Darcy systems*, Numer. Math., 138 (2018), pp. 437–471.
- [7] F. BREZZI, J. DOUGLAS, JR., AND L. D. MARINI, *Recent results on mixed finite element methods for second order elliptic problems*, in Vistas in applied mathematics, Transl. Ser. Math. Engrg., Optimization Software, New York, 1986, pp. 25–43.
- [8] P. D. BRUBECK AND P. E. FARRELL, *A scalable and robust vertex-star relaxation for high-order FEM*, SIAM J. Sci. Comput., 44 (2022), pp. A2991–A3017.
- [9] Z. CAI, R. R. PARASHKEVOV, T. F. RUSSELL, J. D. WILSON, AND X. YE, *Domain decomposition for a mixed finite element method in three dimensions*, SIAM J. Numer. Anal., 41 (2003), pp. 181–194.
- [10] T. CHAUMONT-FRELET AND M. VOHRALÍK, *p -robust equilibrated flux reconstruction in $\mathbf{H}(\text{curl})$ based on local minimizations. Application to a posteriori analysis of the curl-curl problem*, SIAM J. Numer. Anal., 61 (2023), pp. 1783–1818.
- [11] ———, *A stable local commuting projector and optimal hp approximation estimates in $\mathbf{H}(\text{curl})$* . HAL Preprint 03817302, submitted for publication, 2023.
- [12] G. CHAVENT, G. COHEN, J. JAFFRÉ, M. DUPUY, AND I. RIBERA, *Simulation of two-dimensional waterflooding by using mixed finite elements*, Society of Petroleum Engineers Journal, 24 (1984), pp. 382–390.

- [13] L. CHEN, R. H. NOCHETTO, AND J. XU, *Optimal multilevel methods for graded bisection grids*, Numer. Math., 120 (2012), pp. 1–34.
- [14] L. C. COWSAR, J. MANDEL, AND M. F. WHEELER, *Balancing domain decomposition for mixed finite elements*, Math. Comp., 64 (1995), pp. 989–1015.
- [15] L. DIENING, L. GEHRING, AND J. STORN, *Adaptive mesh refinement for arbitrary initial triangulations*. arXiv 2306.02674, 2023.
- [16] W. DÖRFLER, *A convergent adaptive algorithm for Poisson’s equation*, SIAM J. Numer. Anal., 33 (1996), pp. 1106–1124.
- [17] A. ERN AND J.-L. GUERMOND, *Finite elements I—Approximation and interpolation*, vol. 72 of Texts in Applied Mathematics, Springer, Cham, 2021.
- [18] A. ERN AND M. VOHRALÍK, *Stable broken H^1 and $H(\text{div})$ polynomial extensions for polynomial-degree-robust potential and flux reconstruction in three space dimensions*, Math. Comp., 89 (2020), pp. 551–594.
- [19] R. E. EWING AND J. WANG, *Analysis of the Schwarz algorithm for mixed finite elements methods*, RAIRO Modél. Math. Anal. Numér., 26 (1992), pp. 739–756.
- [20] ———, *Analysis of multilevel decomposition iterative methods for mixed finite element methods*, RAIRO Modél. Math. Anal. Numér., 28 (1994), pp. 377–398.
- [21] R. GLOWINSKI AND M. F. WHEELER, *Domain decomposition and mixed finite element methods for elliptic problems*, in First International Symposium on Domain Decomposition Methods for Partial Differential Equations (Paris, 1987), SIAM, Philadelphia, 1988, pp. 144–172.
- [22] F. HECHT, *Construction of a basis at free divergence in finite element and application to the Navier-Stokes equations*, in Numerical solutions of nonlinear problems (Rocquencourt, 1983), INRIA, Rocquencourt, 1984, pp. 284–297.
- [23] W. HEINRICHS, *Line relaxation for spectral multigrid methods*, J. Comput. Phys., 77 (1988), pp. 166–182.
- [24] R. HIPTMAIR AND R. H. W. HOPPE, *Multilevel methods for mixed finite elements in three dimensions*, Numer. Math., 82 (1999), pp. 253–279.
- [25] R. HIPTMAIR, H. WU, AND W. ZHENG, *Uniform convergence of adaptive multigrid methods for elliptic problems and Maxwell’s equations*, Numer. Math. Theory Methods Appl., 5 (2012), pp. 297–332.
- [26] R. HIPTMAIR AND J. XU, *Nodal auxiliary space preconditioning in $\mathbf{H}(\text{curl})$ and $\mathbf{H}(\text{div})$ spaces*, SIAM J. Numer. Anal., 45 (2007), pp. 2483–2509.
- [27] M. INNERBERGER, A. MIRAÇI, D. PRAETORIUS, AND J. STREITBERGER, *hp-robust multigrid solver on locally refined meshes for FEM discretizations of symmetric elliptic PDEs*, ESAIM Math. Model. Numer. Anal., 58 (2024), pp. 247–272.
- [28] M. JAYADHARAN, E. KHATTATOV, AND I. YOTOV, *Domain decomposition and partitioning methods for mixed finite element discretizations of the Biot system of poroelasticity*, Comput. Geosci., 25 (2021), pp. 1919–1938.

- [29] M. KARKULIK, D. PAVLICEK, AND D. PRAETORIUS, *On 2D newest vertex bisection: optimality of mesh-closure and H^1 -stability of L_2 -projection*, *Constr. Approx.*, 38 (2013), pp. 213–234.
- [30] R. B. KELLOGG, *On the Poisson equation with intersecting interfaces*, *Appl. Anal.*, 4 (1975), pp. 101–129.
- [31] R. C. KIRBY, *Low-complexity finite element algorithms for the de Rham complex on simplices*, *SIAM J. Sci. Comput.*, 36 (2014), pp. A846–A868.
- [32] T. P. MATHEW, *Schwarz alternating and iterative refinement methods for mixed formulations of elliptic problems. II. Convergence theory*, *Numer. Math.*, 65 (1993), pp. 469–492.
- [33] A. MIRAÇI, J. PAPEŽ, AND M. VOHRALÍK, *A multilevel algebraic error estimator and the corresponding iterative solver with p -robust behavior*, *SIAM J. Numer. Anal.*, 58 (2020), pp. 2856–2884.
- [34] ———, *A-posteriori-steered p -robust multigrid with optimal step-sizes and adaptive number of smoothing steps*, *SIAM J. Sci. Comput.*, 43 (2021), pp. S117–S145.
- [35] ———, *Contractive local adaptive smoothing based on Dörfler’s marking in a-posteriori-steered p -robust multigrid solvers*, *Comput. Methods Appl. Math.*, 21 (2021), pp. 445–468.
- [36] W. F. MITCHELL, *Adaptive refinement for arbitrary finite-element spaces with hierarchical bases*, *J. Comput. Appl. Math.*, 36 (1991), pp. 65–78.
- [37] W. F. MITCHELL, *The hp -multigrid method applied to hp -adaptive refinement of triangular grids*, *Numer. Linear Algebra Appl.*, 17 (2010), pp. 211–228.
- [38] J.-C. NÉDÉLEC, *Mixed finite elements in \mathbb{R}^3* , *Numer. Math.*, 35 (1980), pp. 315–341.
- [39] P.-A. RAVIART AND J.-M. THOMAS, *A mixed finite element method for 2nd order elliptic problems*, in *Mathematical aspects of finite element methods (Proc. Conf., Consiglio Naz. delle Ricerche (C.N.R.), Rome, 1975)*, Springer, Berlin, 1977, pp. 292–315. *Lecture Notes in Math.*, Vol. 606.
- [40] U. RÜDE, *Fully adaptive multigrid methods*, *SIAM J. Numer. Anal.*, 30 (1993), pp. 230–248.
- [41] R. SCHEICHL, *Iterative solution of saddle point problems using divergence-free finite elements with applications to groundwater flow*, ProQuest LLC, Ann Arbor, MI, 2000. Thesis (Ph.D.)–University of Bath (United Kingdom).
- [42] ———, *Decoupling three-dimensional mixed problems using divergence-free finite elements*, *SIAM J. Sci. Comput.*, 23 (2002), pp. 1752–1776.
- [43] J. SCHÖBERL, J. M. MELENK, C. PECHSTEIN, AND S. ZAGLMAYR, *Additive Schwarz preconditioning for p -version triangular and tetrahedral finite elements*, *IMA J. Numer. Anal.*, 28 (2008), pp. 1–24.
- [44] J. SCHÖBERL AND W. ZULEHNER, *On Schwarz-type smoothers for saddle point problems*, *Numer. Math.*, 95 (2003), pp. 377–399.
- [45] R. STEVENSON, *The completion of locally refined simplicial partitions created by bisection*, *Math. Comp.*, 77 (2008), pp. 227–241.

- [46] S. TAKACS AND W. ZULEHNER, *Convergence analysis of all-at-once multigrid methods for elliptic control problems under partial elliptic regularity*, SIAM J. Numer. Anal., 51 (2013), pp. 1853–1874.
- [47] F. THOMASSET, *Implementation of finite element methods for Navier-Stokes equations*, Springer Series in Computational Physics, Springer-Verlag, New York-Berlin, 1981.
- [48] C. T. TRAXLER, *An algorithm for adaptive mesh refinement in n dimensions*, Computing, 59 (1997), pp. 115–137.
- [49] C. WEBER, *A local compactness theorem for Maxwell’s equations*, Math. Methods Appl. Sci., 2 (1980), pp. 12–25.
- [50] M. F. WHEELER AND I. YOTOV, *Multigrid on the interface for mortar mixed finite element methods for elliptic problems*, Comput. Methods Appl. Mech. Engrg., 184 (2000), pp. 287–302.
- [51] J. WU AND H. ZHENG, *Uniform convergence of multigrid methods for adaptive meshes*, Appl. Numer. Math., 113 (2017), p. 109–123.
- [52] J. XU, L. CHEN, AND R. H. NOCHETTO, *Optimal multilevel methods for $H(\text{grad})$, $H(\text{curl})$, and $H(\text{div})$ systems on graded and unstructured grids*, in Multiscale, nonlinear and adaptive approximation, Springer, Berlin, 2009, pp. 599–659.